Acta Cryst A FOUNDATIONS ADVANCES

ISSN 2053-2733

Response to Fraser & Wark's comments on *A new theory for X-ray diffraction*

Paul F. Fewster*

Brighton, UK. *Correspondence e-mail: paul.f.fewster@gmail.com

Received 26 March 2018
Accepted 17 May 2018

Edited by A. Altomare, Institute of Crystallography - CNR, Bari, Italy

Keywords: diffraction theory; powder diffraction; small crystals.

The criticisms of my theory, as given by Fraser & Wark [(2018), *Acta Cryst.* A**74**, 447–456], are built on a misunderstanding of the concept and the methodology I have used. The assumption they have made rules out my description from which they conclude that my theory is proved to be wrong. They assume that I have misunderstood the diffraction associated with the shape of a crystal and my calculation is only relevant to a parallelepiped and even that I have got wrong. It only appears wrong to Fraser & Wark because the effect I predict has nothing to do with the crystal shape. The effect though can be measured as well as the crystal shape effects. This response describes my reasoning behind the theory, how it can be related to the Ewald sphere construction, and the build-up of the full diffraction pattern from all the scatterers in a stack of planes. It is the latter point that makes the Fraser & Wark analysis incomplete. The description given in this article describes my approach much more precisely with reference to the Ewald sphere construction. Several experiments are described that directly measure the predictions of the new theory, which are explained with reference to the Ewald sphere description. In its simplest terms the new theory can be considered as giving a thickness to the Ewald sphere surface, whereas in the conventional theory it has no thickness. Any thickness immediately informs us that the scattering from a peak at the Bragg angle does not have to be in the Bragg condition to be observed. I believe the conventional theory is a very good approximation, but as soon as it is tested with careful experiments it is shown to be incomplete. The new theory puts forward the idea that there is persistent intensity at the Bragg scattering angle outside the Bragg condition. This intensity is weak ($\sim 10^{-5}$) but can be observed in careful laboratory experiments, despite being on the limit of observation, yet it has a profound impact on how we should interpret diffraction patterns.

1. Introduction

The new theory of X-ray diffraction arose from trying to account for inexplicable experimental observations. Neither the conventional dynamical nor kinematical theories could explain the measurements. The microstructure would have to be fantastical to account for some of these observations. Several experimental examples are included in this article that support the theoretical interpretation. My questioning of conventional theory started in the 1990s when using the near-perfect diffraction space probe (Fewster, 1989) to study polycrystalline materials and perfect semiconductors, with work on a different description beginning in the mid-2000s. It was clear that the observed features could no longer be dismissed as artefacts of the instrument, requiring an alternative explanation of experimental data.

This article is in five sections. The first relates the new theory to the Ewald sphere construction to give a better visual description, which is achieved by simply translating equation (5) of Fewster (2014) into graphical form. The second part describes the build-up of the scattering and where the inten-

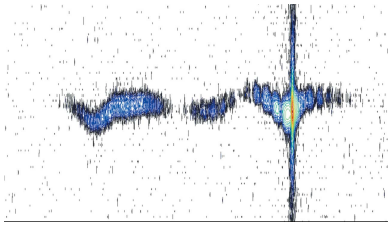

sity is concentrated, including the simple error/misunderstanding/assumption made by Fraser & Wark (2018). The third section gives some experimental evidence of the persistent intensity at the Bragg scattering angle when not in the Bragg condition. The fourth section considers the impact of crystal shape. The fifth section lists some of the examples that are difficult to explain using the conventional theory that are easily explained with the new theory.

2. The relationship of the new theory to the Ewald sphere

The whole basis of the new theory is that a strong scattering feature, *e.g.* a Bragg peak, can still be observed as the crystal is rotated away from its position on the Ewald sphere. This applies to all the diffraction features, *e.g.* thickness fringes and crystal truncation rods, but will be weak. The distance of a diffraction feature from this 'conventional' Ewald sphere surface is given by the length of the arc of a vector (for the feature of interest) rotated about 000 (Fig. 1). The length of the vectors in the figure corresponds to $1/d_{hkl}$. The arcs touch the Ewald sphere at $2\theta_{hkl}$ with a residual amplitude given by equation (4) of Fewster (2014). The next section explains why there is intensity at this position. Thus, a considerable proportion of the full diffraction pattern should be observed if there is sufficient intensity. This is exactly what we would expect from optical diffraction. Rotating the crystal just increases or decreases the intensity of the features in the diffraction pattern, *e.g.* Bragg peaks, thickness fringes, crystal truncation rods, fringes from spherical crystals *etc.*, and when they coincide with the surface of the 'conventional' Ewald sphere the intensity for that feature reaches its maximum value. The 'conventional' Ewald sphere just represents the specular condition and has no width. The new theory just

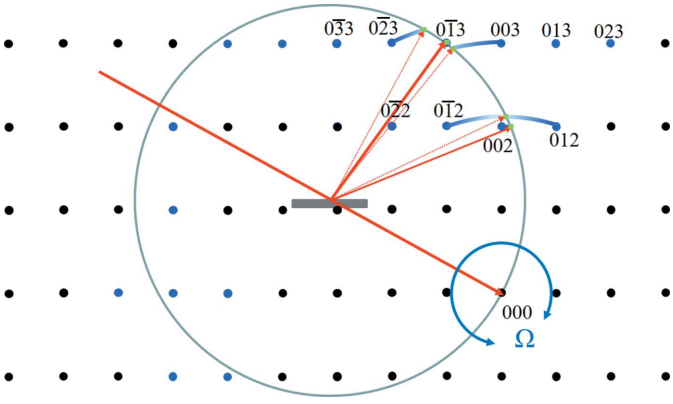

Figure 1
The new theory in terms of the Ewald sphere construction. All the reciprocal-lattice points coloured blue can form intensity at this incident angle at their respective $2\theta_B$ values (*e.g.* green dots) if $0 < \Omega < 2\theta_B$. The distance of the reciprocal-lattice point to the surface of the Ewald sphere along an arc in Ω defines its amplitude, which decreases as the distance increases. For example, 0$\bar{1}$3 is in the Bragg condition and the amplitude is at its maximum value, whereas 002 is weaker and 0$\bar{2}$3 is very weak *etc.* The arcs drawn for some of the reflections give a guide to the strength of the scattering. The Ewald sphere surface can be considered to have a thickness with a profile given by equation (4) of Fewster (2014).

expresses that there is a residual specular contribution that does not go to zero as soon as the feature giving rise to it is rotated away from the optimum position on the sphere surface.

There is also a philosophical question here: if the Ewald sphere has no width then how can a reciprocal-lattice point interact with it? If the crystal is stationary, the source is monochromatic and there is no beam divergence, what would the intensity be? This was a serious problem for Wojtas *et al.* (2017) in their interpretation of XFEL (X-ray free-electron laser) data, requiring the partial capture of a reciprocal-lattice point and invoking angular tolerances to obtain some explanation of the data. If there were too many 'Bragg peaks' then they assumed that they were capturing data from more than one crystal and rejected the data. The new theory defines a width for the sphere surface and this dilemma does not exist. Because it has a width then intensity will be captured away from the Bragg condition. The new theory describes the thickness profile and the associated residual amplitude that is captured.

So, what evidence is there for this? Well there is plenty of evidence, from calculating the diffraction pattern from first principles, results from XFEL sources and even data collected from standard laboratory sources. Let us start with the calculated evidence from my colleague John Anderson and presented by Fewster (2017). This considers a single-wavelength plane wave impinging on a three-dimensional array of point scatterers, which will form a spherical wave from each point. When the scattering is brought together in the far field, *i.e.* the waves travelling in a parallel scattered direction are brought together, a diffraction pattern is formed. The phases of the contributions depend on the difference in path lengths of all the contributions at each 2θ value. The first thing to notice is that the full diffraction pattern exists (Fig. 2*a*). That is not predicted in conventional theory where intensity from a feature only occurs when it touches the surface of the Ewald sphere. This figure is plotted on a logarithmic scale to reveal the detail. For a real experiment the data will have a finite dynamic range and only the strong features are likely to be observed (Fig. 2*b*). These simulations reveal the fringing due to the crystal surface boundary conditions (the shape transform) and if a fringe is close to the Ewald sphere then it could be more intense than the associated Bragg peak that is more remote, *e.g.* Fewster (2016) and Fig. 5 below. These calculations do not contain any complicated parameters (wavelength dispersion or divergence *etc.*), yet the resulting diffraction patterns are very similar to those observed at XFELs, *i.e.* several peaks in an instantaneous image, occasional row of fringes *etc.*, depending on where the dynamic range of these calculations is truncated. The diffraction pattern can be indexed from the $2\theta_B$ of the observed peaks.[1]

Studying these images in greater detail and concentrating on the $2\theta_B$ positions for the Bragg peaks, it is possible to

[1] The peak $2\theta_B$ values were determined with a ruler on the diffraction image and so could only be measured within a few % reliability, because of the peak breadth and the influence of the interference with the fringes, *e.g.* in the vicinity of the 120 peak position.

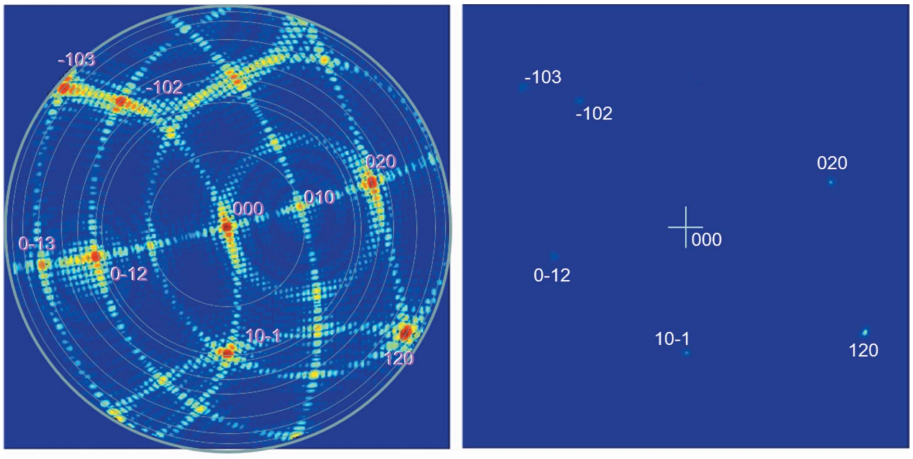

(*a*) (*b*)

Figure 2
The simulation of the diffraction pattern from a three-dimensional array of point scatterers with dimensions 40 × 39 × 40 nm with point separations of 2 × 3 × 4 nm using a wavelength of 1.54 nm. The whole pattern is revealed in a logarithmic plot (*a*). When plotted on a linear scale (*b*) there are six 'peaks' observed. This is very characteristic of data from XFELs. Diffraction based on the conventional theory would reveal nothing in this arbitrary orientation (these are not in the Bragg condition). The central peak in (*a*) is the direct beam and is removed from the linear plot in (*b*), to reveal the other peaks with linear scaling. The plots are displayed on a radius of 2θ out to a maximum of 90°. The peaks can be indexed based on their $2\theta_B$ values and the restriction $0 < \Omega < 2\theta_B$, yet their intensities vary significantly indicating that the reciprocal-lattice points cannot all be close to their Bragg conditions. It can be seen in (*b*) on a linear scale that peak intensities <∼1% of the most intense peak are not observed.

observe intensity enhancement at these angles for this single incident angle. It must be recognized though that there will be peak movements resulting from the interference of the amplitude oscillations related to shape effects and those related to the enhancement effect as Ω is varied. This will also be influenced by how close their contributions are to the surface of the Ewald sphere. The overlap of fringes from reflections of different order will also influence the observed diffraction pattern, which is particularly relevant for small, perfect crystals (Holý & Fewster, 2008; Fewster, 2015, 2018). We can separate out the shape effects by extending the familiar description of Bragg's law.

3. The explanation of the persistent peak at $2\theta_B$ and response to the Fraser & Wark analysis

A series of diagrams (Fig. 3) is given that explains the thinking behind the new theory and the reasoning of Fraser & Wark to make it clear where their misunderstanding has occurred.

A point P_0 on the upper plane will be in phase with any point in any position on the lower plane Q when in the Bragg condition, which in turn will also be in phase with all other points on the upper plane (Fig. 3*a*). When the planes are rotated away from the Bragg condition, the point P_0 will have a close phase relationship with several points on the lower plane, Q_{01}, Q_{02}, Q_{03}, Q_{04} *etc*., and we would expect to see some residual intensity at the specular angle (Fig. 3*b*). The point P_0 can never be exactly in phase with a Q_0 point for this combination of Ω and 2θ outside the Bragg condition (*i.e.* Ω = θ_B). The Fraser & Wark analysis to this point would be the same; then they consider this angular spread of acceptable phases combined with the density of scattering points on the lower plane to give rise to an intensity. I have no dispute with this.

If we now include another point on the top plane, which we call P_1 (Fig. 3*c*), then there will be another set of points on the lower plane that have the same relationship as for P_0. We shall call these points Q_{11}, Q_{12}, Q_{13}, Q_{14} *etc*. These scattering points on the lower plane Q_{1n} will have some overlap with the points Q_{0n}. Since there are as many scattering points on the P and Q planes we should pair every P point with a Q point, and the conclusion would be the same as before if all the P points are in phase (Fig. 3*c*). This arrangement of scattering points produces a peak of intensity at the specular scattering angle that we can call $2\theta_s$. This scattering angle is defined by the crystal surface where the scattered wave exits the crystal and is a result of the boundary condition, which requires the component of the electric field parallel to the surface of the crystal to be continuous. This explains the fringing associated with the crystal shape, often termed the shape transform. If the incident angle is not equal to the Bragg angle, then $2\theta_s$ can never equal $2\theta_B$. This is the conclusion in Fraser & Wark that I agree with; it is purely a conclusion of the conventional theory.

What happens if the detector is moved to a different 2θ angle, whilst maintaining the same incident angle? The description of Fraser & Wark or the conventional theory does not consider this. The scattering does not correspond to the specular condition (Fig. 3*d*) and P_0 is no longer in phase with P_1 and similarly the phase relationship between the scattering from the points P and Q has changed. Conventional theory and that of Fraser & Wark simply assume that intensity only exists when the points P are perfectly in phase. But what happens if the points P scatter slightly out of phase? Is it realistic to assume that there is no intensity in this case? This is a major anomaly in the conventional theory and can be interpreted as the Ewald sphere surface having no thickness.

If we postulate that the points P_0 and P_1 can scatter in a less than perfect phase alignment, then we must conclude that there is intensity outside the specular condition. This has nothing to do with crystal shape. If the detector is moved further the phase relationships between all the P points and all the Q points will change again. Because the phase relationship between all P points can be determined and every P to every Q can be determined, the PQ pair can be paired in an arbitrary way. It is convenient to find the PQ pair that forms a path length difference closest to one wavelength. The phase

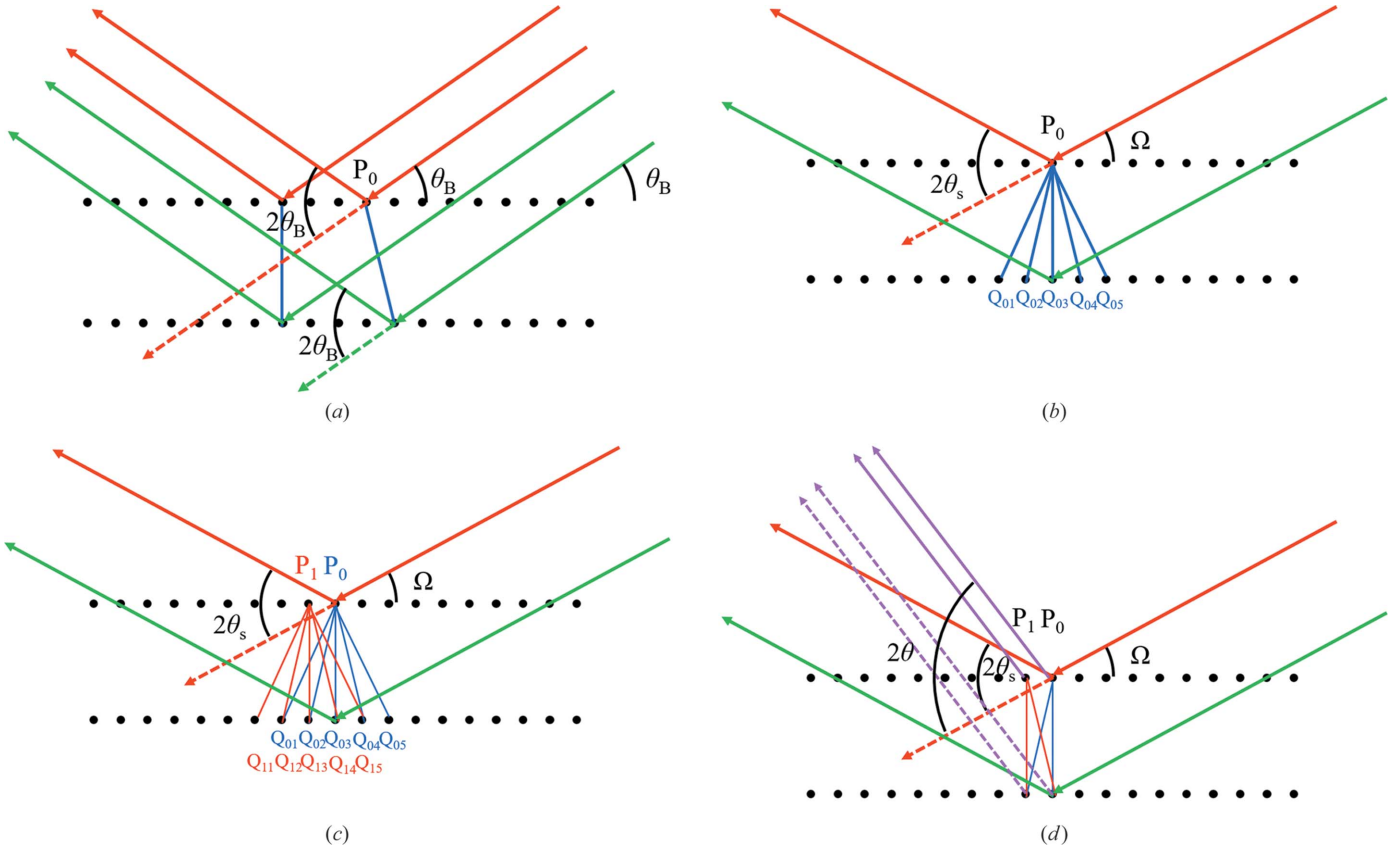

Figure 3
(*a*) The Bragg condition, where all the scattering from all the positions on both planes is in phase, so any pairing of a scattering point from one plane with any point on another plane will be in phase. (*b*) When the scattering planes are rotated away from the Bragg angle a point P_0 cannot scatter in phase with any point Q at the specular scattering angle $2\theta_s$. (*c*) For the same incident angle and the same specular scattering angle the near-phase relationship holds across the plane for P_0, P_1 *etc*. (*d*) However, if we move the detector to a different 2θ, P_0 and P_1 no longer scatter perfectly in phase and similarly the phase relationship associated with P and Q points will change. The phase relationship between the scattering from P and Q points can therefore be varied by moving the detector. If there is a detector position where the path length difference is λ then all the planes will scatter in phase, with a maximum value defined by the phase sum of the amplitudes of points P_0, P_1 *etc*.

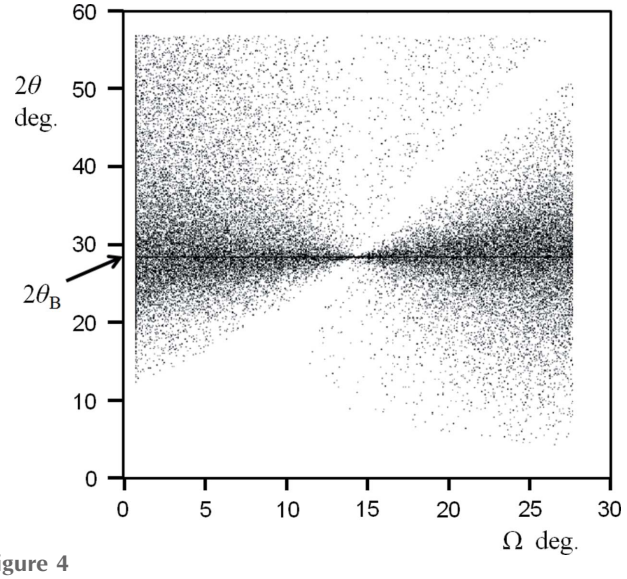

Figure 4
The distribution of path lengths equal to one wavelength (to within a very small tolerance) from scattering points on adjacent planes. As the tolerance is reduced it concentrates on a single value at $2\theta_B$ and the other coincidences become sparser.

difference between P_0, P_1, P_2 *etc*. is determined purely by the incident angle Ω to their plane and the detection point 2θ [equation (4), Fewster (2014)], which defines the maximum amplitude possible from the P plane for this Ω at 2θ, *i.e.* A_Ω. A_Ω applies to the second and all subsequent planes and the maximum amplitude that can exist for this incident angle occurs when all planes scatter in phase with each other, *i.e.* NA_Ω where N is the number of planes. This will only occur if there are PQ pairings that have a path length of one wavelength. By taking a point P on the upper plane and an incident angle Ω, we search for a pairing with a Q position that will give a path length difference of one wavelength by allowing 2θ to take on any value. Fig. 4 is a plot of the angle combinations Ω and 2θ where a one-wavelength path difference can exist between a P position and a Q position. For any given incident angle Ω there is a one-wavelength path difference possible at $2\theta_B$. We can consider that an incident angle below the Bragg angle will form a specular peak at $2\theta_s$ with a maximum path length difference < λ and by increasing 2θ the path length difference can be increased. Similarly, for an incident angle above the Bragg angle a specular peak will form at $2\theta_s$ with a minimum path length difference > λ and by reducing 2θ the

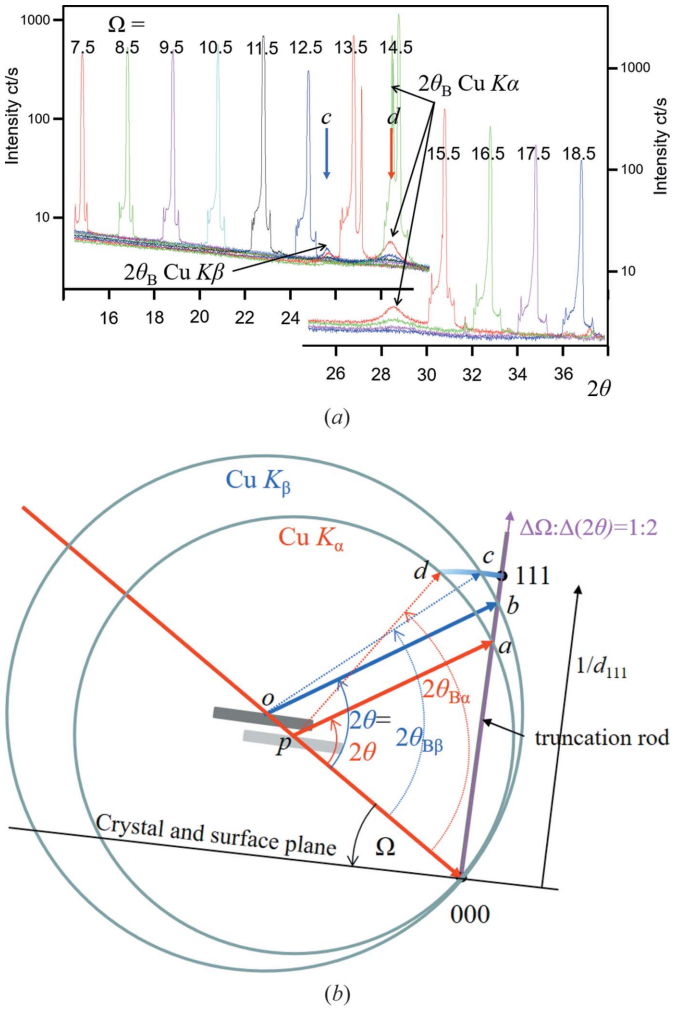

Figure 5
(*a*) Several 2θ scans for fixed Ω settings with the interpretation in (*b*) based on the modified Ewald sphere construction. The spheres have different radii: $1/\lambda_\alpha$ and $1/\lambda_\beta$, centred on *p* and *o*, respectively. Consider the 2θ scan for $\Omega = 12.5^\circ$ in (*a*) (the crystal is orientated 1.7° from the Bragg angle $\theta_{B\alpha}$ for the Cu $K\alpha$ wavelength). There is a single specular peak (the intersection of the 2θ scan and the truncation rod) that is described in (*b*), where the specular contributions occur at the same 2θ but capture different positions on the truncation rod at *a* and *b*, which is the same for both conventional and new theories. The two peaks, *c* and *d*, correspond to the d_{111} plane spacing for both the Cu $K\alpha$ and Cu $K\beta$ wavelengths, *i.e.* $2\theta_\alpha$ and $2\theta_\beta$; in the conventional description these should not exist. The peaks at *c* and *d* can only be described with the new theory, *i.e.* the persistent intensity at $2\theta_\alpha$ and $2\theta_\beta$. The $2\theta_\alpha$ peak can be observed up to $|\Omega - \theta_B| \sim 6^\circ$. The specular peaks are sharp (they are dominated by the proportion of the incident-beam divergence that satisfies this condition, *i.e.* a small region on the sample), and the enhancement peaks are broad (because all the incident-beam divergence directions will form intensity at $2\theta_B$ and these exist over the full footprint of the beam on the sample. As the Bragg condition is approached the peak will sharpen because the strongest contributions come from a smaller range of divergence and smaller regions on the sample and dominate). The features at the base of the specular peaks are tube focus artefacts.

path length difference can be decreased. In both cases we can achieve a path length of λ to form an amplitude of NA_Ω.

This same analysis can be performed for any part of the truncation rod; however, the path length difference never reaches one wavelength but would be associated with a path

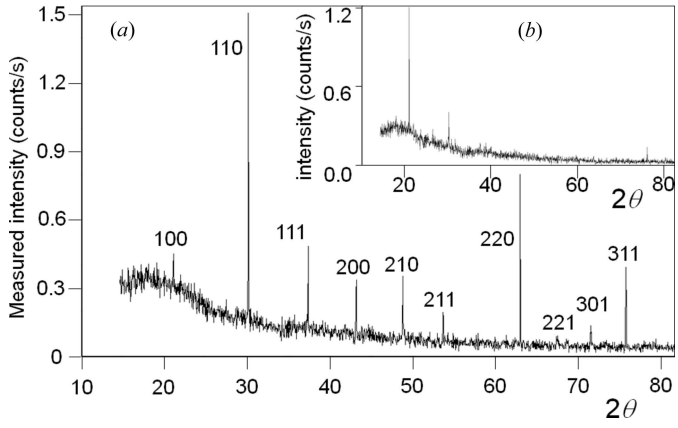

Figure 6
[Fig. 3 from Fewster (2014)]: (*a*) the scattering pattern from ~120 crystals (or if perfectly packed 300 crystals) isolated with a 3.5 μm incident beam that perpendicularly intersects a 1 mm-wide single layer of crystals of LaB_6 with sizes of 2 to 5 μm. (*b*) gives the profile with ~30 crystallites or if perfectly packed 75 crystallites (3.5 μm × 0.25 mm sample size), where only three reflections are clearly resolved compared with all ten in the larger sample size. The data were collected with a 0.01° divergent Cu $K\alpha_1$ beam from a 1.8 kW X-ray laboratory source in 35 min. The samples were stationary throughout, so the incident beam only explored one orientation from each crystal. The peaks are narrow and occur at the correct $2\theta_B$ positions and correspond to the interpretation where each crystal contributes intensity as in Fig. 1.

length above or below this value. The conclusion is that the diffraction pattern is rich with information as in Fig. 2(*a*). This approach ensures that all scattering centres across these planes and by extension all planes in the stack are included.

The new theory therefore predicts that a scan in 2θ over a large range at a fixed incident angle would encounter a peak at $2\theta_s$ corresponding to the specular condition (*e.g.* crystal truncation rod) and at $2\theta_B$ (the enhancement or persistent peak). This is exactly what was observed by Fewster (2016) and further clearer examples are given in the following section, including the measurement of the predicted arc in Fig. 1 [example (iv) in §4].

4. Experimental evidence from laboratory sources

(i) The first example was an early test of my theory. The sample is a large, perfect crystal wafer of 111-oriented silicon. The incident beam (Cu *K*) is collimated to give an angular divergence of 0.03° and the crystal is set to several incident angles, Ω, either side of the 111 Bragg angle (θ_B). The scattering is captured by scanning in 2θ (Fig. 5*a*). Peaks are observed that correspond to the intersection of the crystal truncation rod at $2\theta = 2\Omega$ and further peaks at $2\theta = 2\theta_B$ for both the Cu $K\alpha$ and Cu $K\beta$ wavelengths for the d_{111} crystal planes. The $2\theta = 2\theta_B$ peaks are observed for incident angles up to 6° away from the Bragg condition.

(*a*) How can a crystal set at an incident angle remote from the Bragg condition produce a peak at $2\theta_B$?

(*b*) How can two $2\theta_B$ peaks associated with different wavelengths that require different incident angles be observed simultaneously?

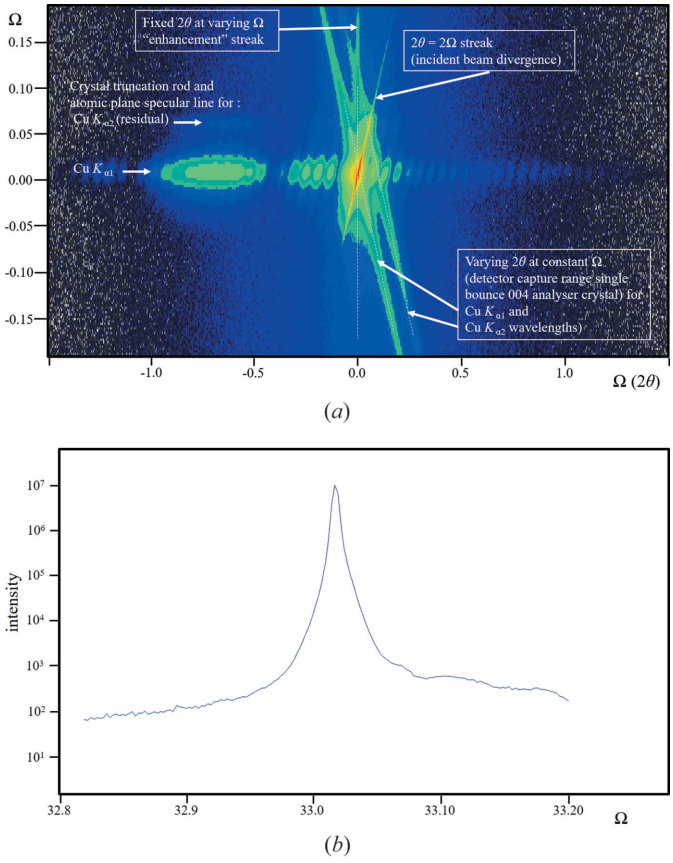

Figure 7
(*a*) A diffraction space map close to the 004 reflection (logarithmic scale) from an InGaAs structure grown epitaxially on a GaAs substrate. The data were collected with the beam selection diffractometer (Fewster, 2004), with a single reflection 004 analyser crystal (stepping in Ω followed by a scan with movements in Ω and 2θ maintaining a 1:2 ratio). The strong fringing is associated with the layer structure (the shape transform) and occurs along the crystal surface normal. The streak where 2θ = 2Ω corresponds to the incident-beam divergence and the streak along 2θ for a constant Ω value corresponds to the detector acceptance range (in this case the diffraction profile of the analyser crystal). The remaining streak at constant 2θ_B for varying Ω values is the 'enhancement' peak for the substrate (as in Fig. 5*b*). (*b*) This is the extracted profile along the 2θ_B enhancement that is smoothly decreasing from the peak as expected, apart from interference of the Cu $K\alpha_2$ streak on the high-angle side. If all the artefacts could be removed and the alignment improved, this could be considered as the thickness profile of the Ewald sphere surface for this reflection and crystal.

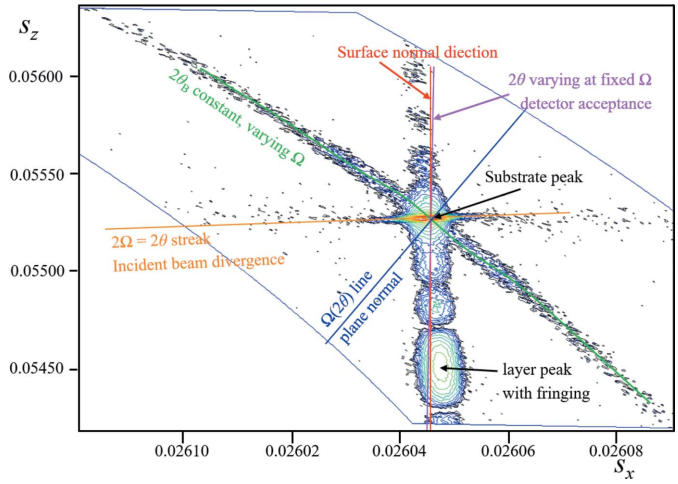

Figure 8
The complex scattering (logarithmic scale) close to the 113 reflection from a Si (001) wafer, with a 46 nm epitaxial layer of $Si_{0.21}Ge_{0.79}$ on top, obtained with a high-resolution diffractometer, courtesy of A. Kharchenko and J. Woitok. The fringing relates to the thickness of the SiGe layer, which can all be explained by conventional (dynamical) theory. The various features determined by the instrument and diffraction geometry are given in the figure and can be related to those in Fig. 7(*a*). The streak of intensity at constant 2θ_B cannot be explained with conventional theory but is predicted by the new theory and corresponds to an arc in Fig. 1.

The explanation based on the new theory is given in Fig. 5(*b*), and because of the large dimension parallel to the surface the shape function is dominated by the crystal truncation rod. The residual peaks at 2θ_B follow the prediction of equation (4), Fewster (2014).

(ii) A very highly collimated monochromatic beam 3.5 µm wide (horizontal with a divergence of 0.01°)[2] is incident on a 1 mm-wide (vertical) polycrystalline sample to form a cross section of 0.0035 mm^2 that is one crystal thick. The average crystal is 3.5 µm in diameter; this illuminated area and absorption measurements (to estimate the packing density) suggest there are ∼120 crystals being illuminated. The sample is kept stationary and the scattering is captured on a position-sensitive detector (the angular spread normal to the scattering plane is limited to 2.3° with a Soller slit). All ten possible peaks at their correct 2θ_B are observed and are sharp (Fig. 6*a*). The probability of capturing one crystal in the Bragg condition is 1 in 23 000, and therefore to capture all ten is 1 in 4 × 10^{43}.

(*a*) How, when the probability of observing a peak at the Bragg condition is 1 in 100 000, can a repeat experiment with ∼30 crystals form three clear peaks (Fig. 6*b*)?

(*b*) Is it reasonable to expect each crystal to be composed of ∼100 000 mosaic blocks?

(*c*) If there are 100 000 mosaic blocks in each crystal, they would have an average diameter of ∼0.075 µm. How can the average intrinsic width for these mosaic blocks (∼0.11°) be reconciled with the measured width of 0.026°?[3]

The new theory has a simple explanation by building all the weak contributions from each crystal as in Fig. 1.

(iii) This is an example of the data from the beam selection diffractometer (Fewster, 2004). This instrument creates very high intensity, near-'zero' wavelength dispersion and well understood instrumental artefacts. The scattering from the sample 004 reflection is captured with a single reflection 004 analyser crystal (Fig. 7*a*). The sample is a perfect crystal. The combination of the analyser crystal and a slit to control the wavelength dispersion still shows the remnants of the Cu $K\alpha_2$ component. In addition to the layer thickness fringes, there

[2] This divergence is based on dynamical theory, and also happens to be the same as the geometrically derived value based on the source size and a crystallite.

[3] This is the measured width, whereas the intrinsic width is ∼0.0025°. An isolated 10 µm Si crystal within a polycrystalline sample (Fewster, 2014) gave a measured width of 0.002°, using a high-resolution diffractometer.

are the influences of the incident-beam divergence and the detector acceptance, which are clearly revealed as streaks emanating from the intense substrate peak. In addition, there is a prominent streak at constant $2\theta_B$. The crystal plane rotation is not accurately normal to the reciprocal-lattice mesh, so this streak is inclined to the plane of the diffractometer.

(*a*) What is the explanation for the streak of intensity at constant $2\theta_B$ as the crystal is rotated in Ω?

The new theory predicts this $2\theta_B$ streak, its shape and how it changes with crystal alignment. Fig. 7(*b*) gives an indication of the intensity along the $2\theta_B$ streak for this sample, *i.e.* 10^{-5} to 10^{-6} of the Bragg peak at an angle of 0.15° from the Bragg condition.

(iv) This example uses a high-resolution monochromator and a position-sensitive detector to study a (001)-oriented Si wafer that has a single $Si_{0.21}Ge_{0.79}$ 46 nm layer grown epitaxially on top. The data were collected close to the 113 reflection by stepping in Ω and scanning in 2θ, and plotted in reciprocal-space coordinates forming an arc of captured data (Fig. 8). The SiGe layer is tilted with respect to the substrate,[4] giving a tilted truncation rod (their individual crystal truncation rods are not coincident but still interfere with each other). The substrate gives rise to the most intense peak and the layer gives a broad peak with fringes. The influence of the incident-beam divergence and the 2θ capture line for a fixed incident angle can all be explained within the description of conventional theory. The substrate is perfect device-grade Si and is not mosaic. There is a very prominent arc of intensity at constant $2\theta_B$ which corresponds exactly to the substrate d_{113} plane spacing. This is the persistent intensity or 'enhancement' predicted by the new theory.

(*a*) Is there any explanation within the confines of conventional theory that can explain this arc of intensity at constant $2\theta_B$ from a perfect crystal as it is rotated in Ω?

This arc of intensity follows the description in Fig. 1 (and discussed later in Fig. 10). It cannot be described by any shape function.

(v) This example is taken from a careful experiment on a structure composed of two epitaxial layers of GaAs/InGaAs on a GaAs substrate. The structure appears to be perfect until it is studied in greater detail with a very high resolution diffractometer (Fewster, 1989) (Fig. 9). There are two significant features that are observed: a crystal truncation rod that 'wiggles'[5] and an intensity streak along $2\theta_B$ associated with the substrate. These features are a common observation in well aligned, good quality crystals, for layer structures and blank crystal wafers. The fringes associated with the layers indicate that the interfaces are flat and parallel. There is interference between the crystal truncation rod for the substrate and the layers, which is only possible if there is significant overlap. The intensity spreading at constant $2\theta_B$ for each part of the structure would account for this overlap and the wiggles.

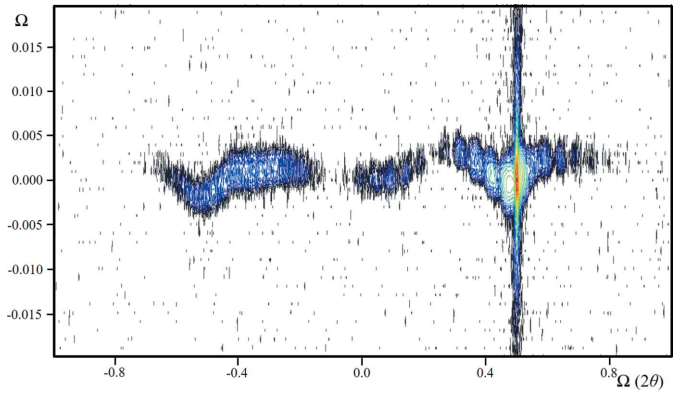

Figure 9
The 004 diffraction space map (logarithmic scale) expanded normal to the crystal truncation rod to emphasize the wavy streak of the 80 Å $In_{0.15}Ga_{0.85}As$ quantum well, buried in a complex AlGaAs/GaAs structure. The other dominant feature is the streak along $2\theta_B$. When the data were projected along $2\theta_B$, the resultant profile fitted precisely with the simulation based on dynamical theory. Collecting data with a high-resolution diffractometer without an analyser (a rocking curve) gave small fringe displacements with a broadened base to the substrate peak (a commonly observed feature, which can be associated with the $2\theta_B$ enhancement for varying Ω), whereas a single scan along the crystal truncation rod gave regions of missing intensity.

(*a*) How can the truncation rods of the substrate and layers interfere without some overlap to create these 'wiggles'?

(*b*) What is the reason for the $2\theta_B$ streak that also gives rise to a broadened base of the substrate peak in an open detector rocking curve?

The new theory predicts the existence of the streak in $2\theta_B$, which in turn will account for the interference of the crystal truncation rods to explain the 'wiggles'. It also indicates how a full two-dimensional diffraction space map can be simulated.

5. The impact of crystal shape

The crystal shape will modify the intensity close to the Bragg peak, which was recognized by Fewster (2014) p. 262: 'Hence a powder sample that has a distribution of orientations will create fringes associated with its size and surface shape and an enhancement at $2\theta_B$ for each crystallite plane'. The main thrust of this theory is to concentrate on the persistent intensity at $2\theta_B$, whereas all shape effects will modify the intensity around the Bragg condition peak and will not form intensity at $2\theta_B$ unless by chance. Equation (5) in Fewster (2014) can be considered as the formula for a crystal wafer with crystal planes parallel to the surface. For other crystal shapes, the full shape transform can be included, but the position of the Bragg condition is unchanged. To include the shape transform for a parallelepiped, as in the work of James (1962) and Authier (2001), for a small crystal, would involve extra terms in equation (5), *i.e.* of the form $\sin(Nx)/\sin x$ and $\sin(Ny)/\sin y$. Since so few crystals conform to this shape I refer to my original statement above, *i.e.* any shape can be included but the persistent intensity at $2\theta_B$ still exists.

[4] This tilt was determined by analysing the 004 reflection at opposite azimuths around the crystal surface normal.
[5] I first considered this to be a problem with the diffractometer; however this is reproduced on different instruments based on different mechanical configurations and scanning arrangements.

To explain the diffraction in the new theory compared with the conventional theory for a parallelepiped, consider Fig. 10 (shape function A), where its shape transform has been simplified to a cross with the tails diminishing in magnitude further from the reciprocal-lattice point. The conventional theory will reveal intensity where the shape transform intersects the Ewald sphere surface, resulting in two peaks. In the new theory the Ewald sphere surface has a thickness given by equation (4) of Fewster (2014). This results in intensity associated with all parts of the shape function and much of it will be very weak. The two peaks as in the conventional theory may well be the most dominant features; however, a strong feature like the maximum in the shape transform will also produce a peak, which may or may not be observed depending on the measurement conditions as in the examples above.

The example given in Fig. 8 has a shape transform like B in Fig. 10 and interacts with a different position on the Ewald sphere surface. The arc of intensity measured corresponds precisely to the prediction in the new theory. More details are given in the caption.

In the new theory, a very small crystal will have a very broad thickness profile for the surface of the Ewald sphere. This increases the observed intensity of features remote from the optimum position on the Ewald sphere surface; so, although the fringing could be touching the optimum position, the main peak in the shape transform can still dominate. This is exactly what is observed in the simulation from a perfect parallelepiped crystal in Fig. 2.

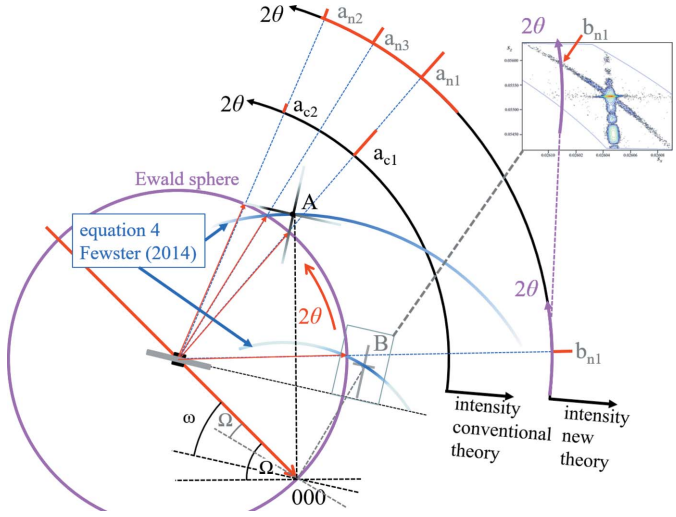

Figure 10
The interaction of different shape functions with the Ewald sphere. A gives rise to peaks a_{c1} and a_{c2} where the tails touch the Ewald sphere; this is the interpretation based on the conventional theory. In the new theory there is another term [equation (4), Fewster (2014)], so that three peaks appear a_{n1}, a_{n2} and a_{n3} (a_{n3} is the enhancement peak) and there is also residual intensity associated with the whole of the shape function. The shape function given at B corresponds to the sample used in Fig. 8, *i.e.* for a crystal wafer with a truncation rod normal to the surface with a very short arm parallel to the surface. At this orientation the conventional theory predicts no peaks since no part of the shape function touches the Ewald sphere. The new theory predicts a peak at $2\theta_B$ (b_{n1}) for all orientations in Ω. The reciprocal-space map B can be compared with the measured data from Fig. 8 (inset) to show how a single extracted 2θ scan away from the Bragg condition forms enhanced intensity at $2\theta_B$.

6. The difficulties with 'conventional theory'

Requiring crystals to be mosaic to suppress dynamical effects (Darwin, 1922) for the kinematical approximation to be applied in structure determination puts a big onus on all crystals. Is that reasonable? The number of crystals required to form a reliable polycrystalline diffraction pattern is greater than in a typical sample, in which case microdiffraction will not work; but it does, so what is going on? This did not go unnoticed by Alexander *et al.* (1948) who suggested crystals in a powder diffraction sample must be mosaic; but how small are they? De Wolff (1958) suggested that slack gearing in diffractometers may be the cause, but high-quality diffractometers of today would rule that out. Smith (1999) concluded that the data cannot be reliable even with the numbers of crystals used in Bragg–Brentano geometry. More recently, the data from XFELs show that there are reflections simultaneously observed in a snapshot from a single crystal, which should be a very rare event but is very common. This has led to a plethora of complex explanations to account for the data, *e.g.* Wojtas *et al.* (2017).

Each explanation is specific to the method by stretching the limits of conventional theory, which is in danger of becoming inconsistent with itself. The descriptions presented by the early workers in this field were valid explanations for their time, but perhaps they cannot be universally applied today. Suppose the fundamental theory is not the complete answer, then the results could be unreliable. Kuhn (2012) would view the conventional theory as a powerful paradigm needing a crisis, *e.g.* inexplicable results, to change it. Have we reached that stage yet? Or can the conventional theory still reveal reliable results? Popper (2002) suggested all theories are waiting to be disproved and therefore should be falsifiable. The assumptions in conventional theory have increased to accommodate these diverse experiments to prevent falsification. This situation is not favoured by the law of parsimony (Occam's razor), which would prefer the theory with the fewest assumptions, because it is easier to falsify.

7. Conclusions

The new theory explains the experimental results. There is, as far as I know, no alternative explanation within the confines of conventional theory. Those who can understand my description as well as the conventional theory should be able to compare these two approaches and make a judgement on which best describes their data. The new theory could be considered as defining a thickness profile for the Ewald sphere surface. In conventional theory this surface has no thickness, placing all the experimental interpretation on changing the shape of the reciprocal-lattice point, *e.g.* mosaic crystals. Shape effects cannot explain the results described above and therefore the conventional theory can only be an approximation. I consider my theory to be a better description of

X-ray diffraction. The criticisms of my theory by Fraser & Wark are therefore based on an invalid argument.

Acknowledgements

I am very grateful to John Anderson for his comments on the manuscript.

References

Alexander, L. (1948). *J. Appl. Phys.* **19**, 1068–1071.
Authier, A. (2001). *Dynamical Theory of X-ray Diffraction*. *IUCr Monographs on Crystallography*, Vol. 11. IUCr/Oxford University Press.
Darwin, C. G. (1922). *London Edinb. Dubl. Philos. Mag. J. Sci.* **43**, 800–829.
Fewster, P. F. (1989). *J. Appl. Cryst.* **22**, 64–69.
Fewster, P. F. (2004). *J. Appl. Cryst.* **37**, 565–574.
Fewster, P. F. (2014). *Acta Cryst.* A**70**, 257–282.
Fewster, P. F. (2015). *X-ray Scattering from Semiconductors and Other Materials*, 3rd ed. Singapore: World Scientific.
Fewster, P. F. (2016). *Acta Cryst.* A**72**, 50–54.
Fewster, P. F. (2017). *IUCr webinar series*, 30th May, IUCr YouTube channel: https://www.youtube.com/watch?v=2sH-6-qwTj0.
Fewster, P. F. (2018). *Acta Cryst.* A**74**, 481–498.
Fraser, J. & Wark, J. (2018). *Acta Cryst.* A**74**, 447–456.
Holý, V. & Fewster, P. F. (2008). *J. Appl. Cryst.* **41**, 18–26.
James, R. W. (1962). *The Crystalline State*, Vol. II, *The Optical Principles of the Diffraction of X-rays*. London: Bell.
Kuhn, T. S. (2012). *The Structure of Scientific Resolutions*. University of Chicago Press.
Popper, K. (2002). *The Logic of Scientific Discovery*. Routledge Classics. Abingdon, Oxford: Routledge.
Smith, D. K. (1999). *Defect and Microstructure Analysis by Diffraction*. *IUCr Monographs on Crystallography*, Vol. 10, edited by R. L. Snyder, J. Fiala & H. J. Bunge, pp. 334–345. IUCr/Oxford University Press.
Wojtas, D. H. *et al.* (2017). *IUCrJ*, **4**, 795–811.
Wolff, P. M. de (1958). *Appl. Sci. Res.* **7**, 102–112.

Acta Cryst A FOUNDATIONS ADVANCES

ISSN 2053-2733

Refuting 'a new theory for X-ray diffraction' – a reciprocal-space approach

Elias Vlieg,* Paul Tinnemans and René de Gelder

Radboud University, Institute for Molecules and Materials, Heyendaalseweg 135, Nijmegen, 6525AJ, The Netherlands. *Correspondence e-mail: e.vlieg@science.ru.nl

Received 16 January 2025
Accepted 28 January 2025

Edited by A. Altomare, Institute of Crystallography - CNR, Bari, Italy

Keywords: X-ray diffraction; scattering theory; crystal termination.

Some ten years ago, Fewster proposed 'a new theory for X-ray diffraction' in order to explain the completeness of powder diffraction patterns from samples with very few crystals, claiming to find extra intensity at Bragg scattering angles $2\theta_B$, even when a grain was not oriented in the Bragg condition, and claiming this to be a new approach to X-ray scattering [Fewster (2014). *Acta Cryst.* A**70**, 257–282]. Fraser & Wark [*Acta Cryst.* (2018), A**74**, 447–456] gave a detailed account of the errors and issues in the approach by Fewster, but the situation appears to be still undecided. To address this issue, we use a different perspective, based on conventional scattering theory and using a simpler description in reciprocal space, rather than the angular space used by Fewster and by Fraser & Wark. This allows us to focus on the crucial conceptual errors in the proposed theory. We show that Fewster is in fact not proposing a new theory, but finds effects that disagree with conventional theory because of errors in the path length calculation. We also discuss extensively the effect of residual intensity in reciprocal space, away from the Bragg peaks, and caused by the termination of crystals. We show that the residual intensity has no significant effect on the intensity of typical powder diffraction patterns. We hope that, with this account, we can put the discussion about the new theory to rest, along with the theory itself.

1. Introduction

In 2014 Fewster published a paper with the title 'A new theory for X-ray diffraction' (Fewster, 2014) (called F14 from now on). The motivation for developing this new theory was the observation that the diffraction from only a small number of crystals can already yield complete powder diffraction patterns. We will present our results on powder diffraction from small samples in a future publication, but here we want to address the ideas put forward in F14. Fraser & Wark (2018) wrote a detailed critique (called FW18 from now on) of the new theory, showing that the claims from F14 are in error. We largely agree with the arguments in FW18 and do not aim to repeat this account. Fewster himself did not agree with FW18, as he expressed in his response (Fewster, 2018*a*) (that we will call F18 from now on) and in a number of subsequent publications (Fewster, 2018*b*; Fewster, 2023). The amount of mathematics and the use of angle parameters in these references may obscure the main arguments, and so part of the X-ray diffraction community may be under the impression that the issue is unresolved. We use a description based on the physics of X-ray scattering and on reciprocal space instead of angular space. The aim of this article is therefore to give as short an account as possible and focus on the key misconceptions and errors; in this way we demonstrate that the new theory is indeed wrong. We are also in a position to address the arguments in F18 and do this where relevant. F14 has, nevertheless, raised a number of interesting points, in parti-

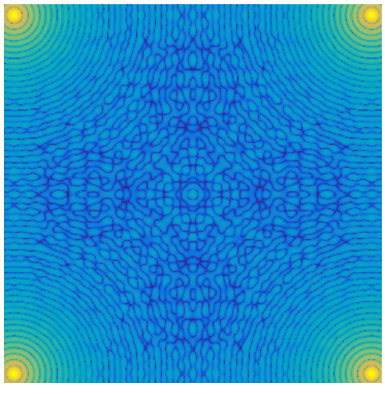

cular concerning the presence and distribution of additional intensity in reciprocal space. This is well known in the conventional theory, and we will show that this residual intensity has no significant effect on the measured intensity of a Bragg peak.

2. The main errors in the new theory

In the *Introduction* of F14, it is stated that 'An alternative viewpoint is presented here, where the whole of diffraction space is occupied by scattering from many crystal planes, which when combined contribute to the peaks observed'. We agree with this description of diffraction, but stress that this is standard X-ray scattering theory and not an alternative viewpoint. Nevertheless, using this same basic methodology, F14 should have arrived at the same result as the conventional theory if applied correctly. We will first show that the amplitude derived in F14 is wrong, then point out the mistakes in the path length calculation that lead to the wrong amplitude, and finally emphasize the major misconception that resulted from this and that formed the basis of the new theory.

2.1. The scattering amplitude

In F14 a 2D model for a crystal is used, in which the lattice planes are represented as planes (lines to be precise) of uniform electron density. The conventional theory yields for this case the following expression for the scattering amplitude:

$$A'(h,k) = \frac{\sin(\pi N_a h)}{\pi h}\frac{\sin(\pi N_b k)}{\sin(\pi k)}. \tag{1}$$

Here h and k are the diffraction indices that can have *real* (not only integer) values and N_a and N_b are the number of unit cells along the crystallographic a and b directions. Section $A1$ of the Appendix gives a summary of conventional theory, and we refer to this for details on the derivation of the scattering amplitude. F14 does not use diffraction indices to represent a specific scattering geometry, but incoming and outgoing angles with respect to the scattering planes, and therefore we will need to convert equation (1) to the angular coordinates used in F14. Fig. 1 shows the geometry and scattering angles. It is straightforward to show that the following relation holds:

$$\begin{pmatrix} h \\ k \end{pmatrix} = \frac{a}{\lambda}\begin{bmatrix} \cos(2\theta-\Omega)-\cos\Omega \\ \sin(2\theta-\Omega)+\sin\Omega \end{bmatrix}, \tag{2}$$

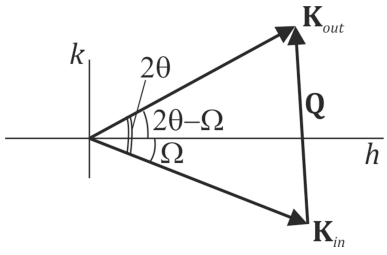

Figure 1
The incoming and outgoing wavevectors, oriented such that the total scattering angle is 2θ. The incoming angle is Ω.

where a is the lattice constant, λ the wavelength, Ω the incoming angle and 2θ the scattering angle. We refer to Section $A2$ of the Appendix for details. Substituting the full expressions for h and k in equation (1), we obtain

$$A'(\Omega,2\theta) = \frac{\sin\left\{\frac{\pi N_a a}{\lambda}[\cos(2\theta-\Omega)-\cos\Omega]\right\}}{\frac{\pi a}{\lambda}[\cos(2\theta-\Omega)-\cos\Omega]} \times \frac{\sin\left\{\frac{\pi N_b a}{\lambda}[\sin(2\theta-\Omega)+\sin\Omega]\right\}}{\sin\left\{\frac{\pi a}{\lambda}[\sin(2\theta-\Omega)+\sin\Omega]\right\}}. \tag{3}$$

This expression is, as it should be, the same as that presented by FW18 as equation (5), except that they did not use the diffraction plane approximation and thus have a sine term in the left-most denominator. Both equation (1), using diffraction indices, and equation (3), using angular coordinates, are based on conventional theory and cover all possible scattering geometries. F18 thus clearly makes a mistake by stating 'What happens if the detector is moved to a different 2θ angle, whilst maintaining the same incident angle? The description of Fraser & Wark or the conventional theory does not consider this'. This is not true, the conventional theory *does* consider this.

Now we compare our result with equation (F14-5). The first part of equation (F14-5) is the same as equation (F14-4), which we copy here for convenience:

$$A_{\Omega,\mathrm{F14}} = \frac{\sin\left\{\frac{\pi L_x}{\lambda}[\cos(2\theta-\Omega)-\cos\Omega]\right\}}{\left\{\frac{\pi L_x}{\lambda}[\cos(2\theta-\Omega)-\cos\Omega]\right\}}. \tag{F14-4}$$

Note that $L_x = N_a a$. It is nearly the same as the first term in equation (3), except that the denominator contains an L_x term that should not be there. This gives a much lower amplitude, but otherwise does not affect the behaviour as a function of the angles 2θ and Ω. Equation (F14-4) was not derived in F14, so it is unclear why the L_x term is present, but it might be a simple typing error. Except for this detail, the equations agree and this shows that the conversion from diffraction indices to angles works properly. The significant differences, however, are found in the second term, describing the interference between planes. We copy this part of equation (F14-5) for convenience as well:

$$A_{2\theta,\mathrm{F14}} = \frac{\sin\left(\frac{\pi d}{\lambda}2\sin\theta - n\pi\right)}{\left(\frac{\pi d}{\lambda}2\sin\theta - n\pi\right)}\frac{\sin\left[N\left(\frac{\pi d}{\lambda}2\sin\theta - n\pi\right)\right]}{\sin\left(\frac{\pi d}{\lambda}2\sin\theta - n\pi\right)}. \tag{F14-5}$$

For the comparison, we should use $d = a$ and $N = N_b$. The n in this equation corresponds to a path length difference of multiple wavelengths. While there are similarities, the differences are profound and the two terms clearly do not agree with each other. We claim the expression we use is the correct

one because (i) it is based on a standard result that can be found in several textbooks; (ii) it is essential in the computation to add all the contributions with the correct phase and this is guaranteed in our case by using the standard expressions for path length difference. In F14, however, the phases are calculated in an elaborate, but incorrect way, as explained by FW18 and in our next section. It is unfortunate that F18 does not contain a response to the mathematical errors and arguments as pointed out by FW18, nor provide more details on how equation (F14-5) was derived. We conclude, as did FW18 before us, that the scattering amplitude used in F14 is wrong.

2.2. Path length difference

At the Bragg condition, where the scattering angle has the value $2\theta_B$ and $\Omega = \theta_B$, the scattering amplitudes from all parallel planes are in phase. (This is true for a series of n angles, following Bragg's law $2d \sin\theta = n\lambda$, but we will use $n = 1$ as 'the' Bragg angle.) In order to demonstrate that two parallel planes can be in phase when $\Omega \neq \theta_B$, F14 computes the path length difference for a point on the top plane and a point on the next lower plane that is laterally displaced by a distance x. Fig. 2 shows the geometry used. In F14 the following value is found for this path length difference:

$$\Delta(x) = d[\sin\Omega + \sin(2\theta - \Omega)] - x[\cos\Omega - \cos(2\theta - \Omega)], \tag{4}$$

and we agree with this expression. A full calculation of the amplitudes based on this value would have given the conventional result, thus equivalent to the amplitude derived in reciprocal-space coordinates in the Appendix. The mistake that F14 makes is to demand ('and must also be satisfied') that this path length difference should be equal to

$$\Delta_{0,\mathrm{F14}} = 2d \sin\theta, \tag{5}$$

stated to be 'the condition when $x = 0$'. Demanding that these path length differences are the same means that

$$d[\sin\Omega + \sin(2\theta - \Omega)] - x[\cos\Omega - \cos(2\theta - \Omega)] = 2d \sin\theta. \tag{6}$$

This is *only* true for $\Omega = \theta$. The true value for $x = 0$ follows directly from equation (4):

$$\Delta_{x=0} = d[\sin\Omega + \sin(2\theta - \Omega)]. \tag{7}$$

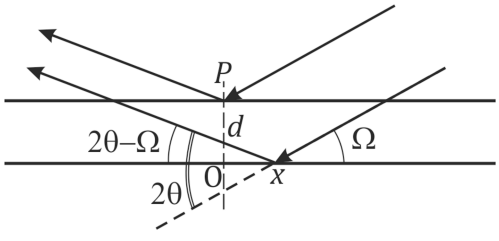

Figure 2
The scattering geometry for computing the path length difference between point P on the top plane and a point x on the lower plane. O is the origin on the lower plane. This is an adaptation of Fig. 4(d) from F14.

The values for $\Delta_{0,\mathrm{F14}}$ and $\Delta_{x=0}$ are again *only* equal when $\Omega = \theta$. We fail to understand why this specific condition is needed, nor why one would expect Δ, which is found to be a function of x, to ever have the same value as at the point $x = 0$. As already stated, the only exception for this is when $\Omega = \theta$, but the exercise is explicitly meant for conditions $\Omega \neq \theta$. This is simply wrong. FW18 already notes this as the 'first of the major errors' in F14, but viewed this as an unjustified mathematical approximation. We consider this to be the conceptual error. Requiring Δ to be equal to $n\lambda$ would make sense, because then the two points are in phase as was stated to be the aim of the computation, but that is not what F14 uses.

It is unclear how the erroneous path length difference leads to equation (F14-5), because no details are presented; but it is clear that the path length error explains the error in the final calculated amplitude, as discussed above. In the next section we will show how the path length difference can be calculated correctly, including the condition that parallel planes are in phase. We also show what the consequences are of the mistakes of F14.

2.3. No local maxima at $2\theta_B$

Using the wrong expression for the amplitude, F14 comes to the conclusion that there is a peak in intensity at the Bragg scattering angle $2\theta_B$, even when $\Omega \neq \theta_B$, thus even when not at the Bragg condition. According to F14, this occurs because, at this condition, the parallel planes scatter in phase. We quote: 'It is important to show that the scattering from a stack of parallel planes remains in phase when $\Omega \neq \theta_B$ at the scattering angle $2\theta_B$'. We will show that this is wrong and consider this to be the main misconception on which the new theory for X-ray diffraction was based.

To keep the discussion and mathematics simple, we will use the description using diffraction indices [equation (1)]. As discussed above, in F14 the phase difference between parallel planes is computed and a lateral distance x is introduced for which a point on the top plane is in phase with the underlying one. The argument in F14 is that when this is true for those two points, it will be true for all pairs of points and thus the planes are in phase. It is true that the planes can be in phase, but this does *not* occur at the Bragg scattering angle $2\theta_B$ (except for the Bragg peak itself, when $\Omega = \theta_B$). The condition for which the planes are in phase can be directly determined by using equation (1). The geometry we are considering corresponds to the 01 reflection in this 2D case. When we keep k at the value 1, then there is indeed no phase difference between parallel planes and the amplitude is N_b times the contribution of a single plane:

$$A'(h, k = 1) = N_b \frac{\sin(\pi N_a h)}{\pi h}. \tag{8}$$

Equation (1) shows that the profile has a sharp maximum for $k = 1$, for any value of h. This local maximum thus occurs as a *straight* line in reciprocal space along the h direction. The value of the local maximum rapidly decreases away from the Bragg peak. (In Section 3 we will show that the local maximum

is a feature specific for the parallelepiped crystal shape considered here.)

The mistake in the path length difference in F14 leads to the erroneous result that the condition of perfect constructive interference between the planes corresponds to the condition that the scattering angle should be $2\theta_B$. Using diffraction indices, this angular condition of F14 means that the length of the scattering vector should be 1. (The argument remains the same if we choose a different integer value for this diffraction index.) We can satisfy this by requiring $(h, k) = (\sin\sigma, \cos\sigma)$, with σ an angle that represents the deviation from the Bragg condition. The trajectory of (h, k) is thus a *circle* in reciprocal space and not the straight line at $k = 1$ we found above. In short, F14 assumes that local maxima occur when (h, k) follows a circular trajectory, while in reality this occurs along a straight line for which 2θ varies. Fig. 3 graphically shows the difference in these in-phase conditions. Very close to a Bragg peak, a circle is an excellent approximation of the straight line, but this circle is *not* the correct condition for constructive interference between the parallel planes. We note that Fig. 13 of FW18 illustrates the same issue, be it in angular coordinates.

Along this circle, the amplitude is

$$A'(\sigma) = \frac{\sin(\pi N_a \sin\sigma)}{\pi \sin\sigma} \frac{\sin(\pi N_b \cos\sigma)}{\sin(\pi \cos\sigma)}. \qquad (9)$$

The right-most term shows that, for increasing values of σ (moving away from $\Omega = \theta$), the planes are increasingly out of phase. This has two important consequences: (i) there is *no* local amplitude maximum at the scattering angle $2\theta_B$, because this maximum moves to larger 2θ values when moving away from the Bragg peak, and (ii) there is *no* accumulation of significant intensity at the scattering angle $2\theta_B$ when a crystal is not oriented at the Bragg condition.

By considering a 2D case, with the amplitude as given in equation (1), F14 ignores another aspect of the intensity in reciprocal space. There is a local maximum along a straight *line* for $k = 1$ in this model. As will be discussed in more detail in the next section, for a 3D, cube-shaped crystal, a local maximum occurs any time two of the diffraction indices are integer, and thus the local maxima continue to occur along a *line*, also for the 3D case. In the 2D case a small fraction of grains of a powder sample may have the correct orientation to correspond to a local maximum, but in the 3D case with the additional degree of freedom, the fraction is much lower. The 2D case discussed in F14 thus creates the wrong impression of the actual situation in 3D.

We conclude that the ideas put forward in F14 are based on an error in the path length calculation and that the computation method corresponds to standard scattering theory. It is not a new theory for X-ray diffraction, but the conventional one, wrongly applied.

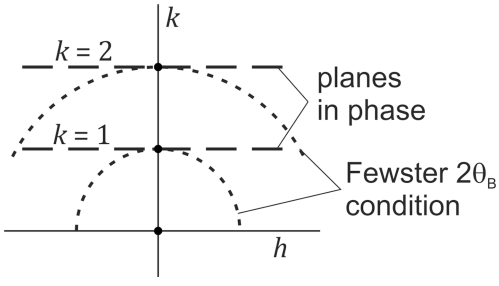

Figure 3
A schematic of reciprocal space showing the conditions for which the contributions of the parallel planes are in phase. This occurs for integer values of the diffraction index k. In F14, the in-phase condition is erroneously computed to lie along a circle.

3. Crystal termination

We have found that in general there is no local amplitude maximum for the scattering angle equal to $2\theta_B$, but there is certainly some intensity all over reciprocal space, away from the Bragg condition. This is predicted by conventional diffraction theory and equation (1) gives the amplitude for the 2D case when using planes instead of lattice points. In order to discuss the effect of the additional intensity, we will use the more realistic case of a 3D lattice. The derivation is done in Section *A*1 of the Appendix, with as result:

$$I(\mathbf{Q}) = \frac{\sin^2(\pi N_a h)}{\sin^2(\pi h)} \frac{\sin^2(\pi N_b k)}{\sin^2(\pi k)} \frac{\sin^2(\pi N_c l)}{\sin^2(\pi l)}. \qquad (10)$$

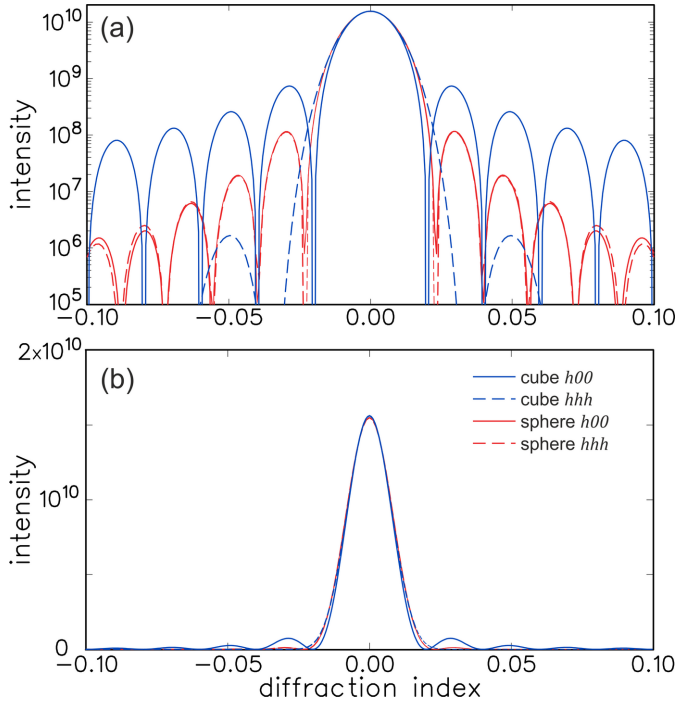

Figure 4
The intensity from a cubic crystal with a size of 50 unit cells (blue curves) and a spherical crystal with a radius of 31 unit cells (red curves). (*a*) Plotted on a log scale and (*b*) plotted on a linear scale. The graphs represent the intensity along the *h*00 and the *hhh* directions in reciprocal space. For the cubic crystal, these two intensities are very different, but for the spherical one they are nearly the same. On the log scale the secondary maxima appear significant, but the linear scale shows that these are very small.

Here we left out pre-factors that are not important for this discussion. Note that we do not use the amplitude here, but the intensity. We will now discuss the significance of this intensity for a powder diffraction pattern. For simplicity, we will assume we have a crystal with a cubic shape and lattice.

Equation (10) gives very strong peaks when *hkl* are all integer, thus at the Bragg reflections. The equation also yields secondary maxima, where the strongest ones are found when two of the diffraction indices have integer values (meaning that along those directions the scattered waves are all in phase). This leads to spikes of intensity along the reciprocal-lattice axes, representing *local* maxima. For this specific crystal, these local maxima thus occur along six directions away from a Bragg peak. Along the *a* direction, for example, the first secondary maximum is at a distance $\Delta h \approx 1/N_a$ from the maximum and has a height that is a factor ~ 20 lower than the true maximum. Fig. 4 shows a plot along this direction for the case of $N_a = N_b = N_c = 50$ and k, l both integer, thus along the *h*00 direction in reciprocal space (solid blue curve). (For the cubic crystal considered here, the *h*00 direction in reciprocal space is the [100] direction in real space; in general the spikes will be perpendicular to the crystal facets.) For normal crystals, there are many unit cells and thus this secondary maximum is located very close to the main peak. Only in special circumstances can one observe these fringes, because almost always the angular and wavelength spread of the X-ray source will wash them out. (For thin films, where the number of layers can be very small, such fringes can be observed.) More importantly, however, is the fact that the intensity according to equation (10) is for the special case of a crystal with a very sharp termination along all six facets, leading to relatively strong maxima perpendicular to the facets. To illustrate the effect of these facets, the figure also shows the intensity along the *hhh* direction (dashed blue curve), thus not corresponding to a facet of this cubic shape. As expected, along this direction, the intensity is much weaker.

An alternative illustration of these effects is shown in the top half of Fig. 5, where the intensity is plotted along a plane in reciprocal space. (A similar plot was presented in FW18.) The increased intensity when two of the diffraction indices are integer is clearly visible using a log scale. When plotted on a linear scale, however, the residual intensity is found to be very weak, even for this very small crystal. This was already visible more quantitatively in the line plots of Fig. 4.

The effect of the presence of well defined facets can be further illustrated by considering an alternative simple crystal form: a sphere. A sphere with a cubic lattice and with a radius of $N_R = 31$ unit cells has the same volume as the 50 unit cell cube, so we use this size for comparison. The amplitude is now found from the summation

$$A_{\rm sphere}(h,k,l) = \sum_{n_a,n_b,n_c}^{n_a^2+n_b^2+n_c^2 \le N_R^2} \exp[2\pi i(n_a h + n_b k + n_c l)]. \quad (11)$$

Because of the coupling of the three directions, this does not yield a simple intensity formula, but the summation can easily be done numerically. Fig. 4 plots the corresponding intensity for the *h*00 and *hhh* directions in reciprocal space (red curves). There are two main differences with respect to the cube: (i) the secondary maximum is much lower than for the cubic *h*00 direction (~ 130 times weaker than the value of the main peak) and (ii) the *h*00 and *hhh* directions are now (nearly) equal. Both features arise from the fact that a sphere has no (large) facets and thus the secondary maxima are (nearly) equal in all directions and not peaked in any particular direction. While the secondary maxima are clearly visible in the log-scale plot, the linear scale shows that the secondary maxima are negligible compared with the real maximum and can thus be ignored. These conclusions are confirmed by the 2D intensity plot for the spherical crystal in Fig. 5. We note that also for the spherical crystal, the scattering amplitudes from different planes are in phase for integer values of the corresponding diffraction indices, but because of the shape, these directions do not lead to local maxima in reciprocal space. FW18 already discussed the case of a spherical crystal, using a description in angular coordinates.

Both a perfect cube and a perfect sphere are of course unrealistic representations of 'normal' crystals. When the shape is irregular, the secondary maxima are even weaker compared with the primary maximum. Besides the fact that the grains of a powder sample will typically have an irregular shape, they also have dimensions of some 10000 unit cells in all directions. This strongly reduces the residual intensity

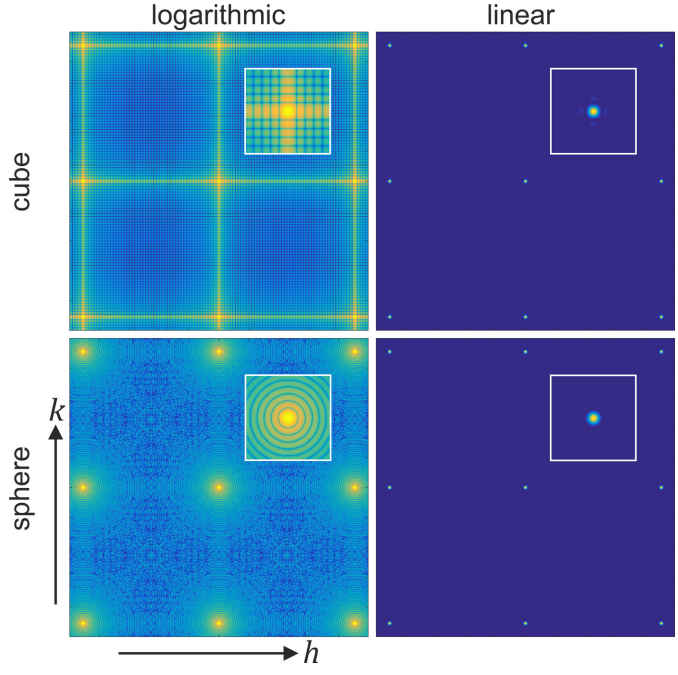

Figure 5
The intensity of crystals with cubic (top) and spherical (bottom) shape, plotted in the h, k plane, and with l having an integer value. The sizes of the crystals are the same as in Fig. 4. For the cubic crystal, the intensity shows local maxima connecting the Bragg peaks, but this disappears for the spherical crystal. The plots using a logarithmic scale (left) clearly show the intensity distribution, but the linear scale (right) gives a more realistic idea of the residual intensity compared with the main peaks. The insets are an enlarged view of a single Bragg reflection.

compared with the main peak, especially for crystals without large facets. We refer to Section *A*3 of the Appendix for details.

The secondary maxima will in general be further suppressed by the fact that typical surfaces will be rough. This is already somewhat illustrated in Fig. 4, because a sphere can ('roughly') be considered as a very rough version of a cube. A good and general way to demonstrate the effect of roughness is to use the so-called crystal shape function. The effect of surface roughness is a well known issue in the field of surface X-ray diffraction (Robinson & Tweet, 1992; Vlieg, 2012), where roughness can hamper the measurement of so-called crystal truncation rods (Robinson & Tweet, 1992). These rods are the equivalent of the intensity spikes of the cubic crystal, but without the fringes. The fringes are a finite-size effect, but crystal truncation rods occur also for half-infinite crystals, showing that the residual intensity can more generally be considered a crystal termination effect. Roughness will reduce the intensity near the Bragg peak by at least another factor 10. We refer to Section *A*4 of the Appendix for more details.

All these arguments show that the residual intensity, away from the Bragg condition, from a grain will be very low, of the order of 10^{-6} compared with the main peak. Having a powder with 1 million grains then might appear to still give significant intensity that will be added to the measured integrated intensity. However, this is not the case, because the crystals have random orientations and the intensity is distributed uniformly (for an ideal powder) over a sphere in reciprocal space. Only a small fraction of this will be in the part of the Debye–Scherrer ring that is observed. The integration of the intensity over all these grains at one specific observation direction is equivalent to the integration over the full reciprocal space of one grain. As we saw, only very close to the Bragg peak is there some intensity, but it is very weak. This means that the extra intensity remains at the level of 10^{-6}. In F14, one of the motivations to explore the new theory was the observation of (quite) complete powder diffraction patterns from samples with about 300 grains. We have shown that the termination effects cannot explain this, but will come back to this interesting point in a future publication.

On individual grains, with the right size and shape and using a wide dynamic range, the tails (and even fringes) can be observed, and F18 shows some examples. This does not mean, however, that this intensity is significant for powder X-ray diffraction. We note that in F18, Fewster states (in his abstract) that the extra intensity is $\sim 10^{-5}$. Fewster puts the intensity in the wrong place in reciprocal space, but the value mentioned in F18 agrees roughly with our estimates. In F14, however, the total contribution of the non-Bragg intensity at $2\theta_B$ was estimated as 30%, but that is clearly in disagreement with the 10^{-5} estimate Fewster made later, and also with our estimate.

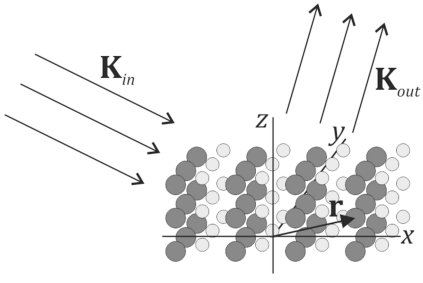

Figure 6
A schematic of the geometry when X-rays scatter from a crystal. The incoming and outgoing X-ray beams are assumed to be plane waves, represented by the wavevectors $\mathbf{K}_{in}$ and $\mathbf{K}_{out}$, respectively. The scattering amplitude is obtained by summing over the contributions from all atoms.

Based on the wrong idea that conventional theory does not consider scattering from all crystal planes, F18 claims that FW18 have misunderstood the concept and methodology used in F14. F18 states that the new theory 'only appears wrong to Fraser & Wark because the effect I predict has nothing to do with the crystal shape'. We want to stress here the point we have demonstrated above: when including the scattering from all planes, the resulting amplitude *does* depend on the crystal termination and thus on the crystal shape, because the planes have to end somewhere.

4. Conclusions

The 'new theory for X-ray diffraction' proposed by Fewster in 2014 is not new, but uses the standard methodology of X-ray scattering. Because of a conceptual error in the calculation of the path length difference, the application of the theory led to the wrong conclusion that there is a local maximum in scattered intensity at the Bragg scattering angle $2\theta_B$, even from a crystal oriented away from the Bragg condition.

There is residual intensity in reciprocal space, away from the Bragg peaks, because of the termination of a crystal. The location and magnitude of this intensity depend on the size and shape of a crystal. Except for very special circumstances, the residual scattering does not give a significant intensity enhancement at the Bragg peaks in the case of powder X-ray diffraction. We thus have to discard the new theory and can continue to use the conventional one.

APPENDIX *A*

A1. Kinematic scattering

We describe in some detail how the diffracted intensity from a crystal can be calculated. We present this for convenience to have all results at hand in a concise way, but do not claim any originality; the concepts discussed in this section can be found in standard textbooks. We use the perspective of X-ray scattering theory, which is somewhat different from the typical approach used by crystallographers, but the final results are the same. For the X-ray scattering approach we refer to the excellent treatments by Guinier (1994) and Cowley (1984). The crystallography approach can be found for example in the books by Warren (1990), Giacovazzo (2011) and Hammond (2015).

For small crystals, the scattering of X-rays is accurately described using the single-scattering approximation, also known as kinematic scattering. This means that the X-rays that

are scattered from atoms are assumed not to scatter again. Since the scattering cross section of X-rays is very small, this is in most cases an excellent approximation. We further assume that we have a 'perfect' crystal, *i.e.* we ignore defects, because this is irrelevant for the issues we aim to address. When assuming, in addition, that the X-ray source and X-ray detector are at a large distance from the crystal, the incoming and outgoing beams can be described by plane waves. Then the so-called scattering amplitude can be written as

$$A(\mathbf{Q}) = r_e \int \rho(\mathbf{r}) \exp(i\mathbf{Q}\cdot\mathbf{r})\,\mathrm{d}\mathbf{r}, \tag{12}$$

with r_e the classical electron radius, $\mathbf{Q} = \mathbf{K}_{\rm out} - \mathbf{K}_{\rm in}$ the momentum transfer, $\rho(\mathbf{r})$ the electron density and $\mathbf{r}$ a position within the crystal (with respect to a fixed origin). Fig. 6 schematically shows the scattering geometry. The length of the wavevectors is $|\mathbf{K}| = 2\pi/\lambda$, with λ the wavelength. The scattering amplitude is the summation (integration) of the contributions of all atoms with the appropriate phase factor, given by $\mathbf{Q}\cdot\mathbf{r}$. Mathematically, the amplitude is the Fourier transform of the electron density. The incoming ($\mathbf{K}_{\rm in}$) and outgoing ($\mathbf{K}_{\rm out}$) wavevectors are plane waves. Note that no assumption is made (yet) concerning the angles of the incoming or final wavevectors with respect to the crystal.

For a crystal, the atoms are located at well defined positions, as given by (i) the arrangement of the atoms within a unit cell and (ii) the periodic stacking of the unit cells according to the crystal lattice parameters a, b and c. In general, we can write the position of unit cell j as

$$\mathbf{R}_j = n_a\mathbf{a} + n_b\mathbf{b} + n_c\mathbf{c}, \tag{13}$$

with n_a, n_b and n_c integer values. The integral in equation (12) can thus be replaced by a summation over all unit cells and an integration over the electron density $\rho_u(\mathbf{r})$ of a single unit cell:

$$A(\mathbf{Q}) = r_e F(\mathbf{Q}) \sum_{n_a,n_b,n_c} \exp(i\mathbf{Q}\cdot\mathbf{R}_j), \tag{14}$$

with

$$F(\mathbf{Q}) = \int \rho_u(\mathbf{r}) \exp(i\mathbf{Q}\cdot\mathbf{r})\,\mathrm{d}\mathbf{r}. \tag{15}$$

The summation in equation (14) can conveniently be performed by writing $\mathbf{Q}$ as a vector in reciprocal space:

$$\mathbf{Q} = h\mathbf{a}^* + k\mathbf{b}^* + l\mathbf{c}^*, \tag{16}$$

and where we explicitly allow the diffraction indices h, k and l to be real numbers, thus not restricted to integer values. $\mathbf{a}^*$, $\mathbf{b}^*$ and $\mathbf{c}^*$ are the reciprocal-lattice vectors. Using this, the summation becomes

$$\sum_{n_a,n_b,n_c} \exp(i\mathbf{Q}\cdot\mathbf{R}_j) = \sum_{n_a,n_b,n_c} \exp[2\pi i(n_a h + n_b k + n_c l)]. \tag{17}$$

The result of this summation depends of course on the size and shape of the crystal. For simplicity, we start with a crystal in the form of a parallelepiped with N_a, N_b and N_c unit cells along the three crystal axes, respectively. The summation then becomes

$$\sum_{n_a=0}^{N_a-1} \exp(2\pi i n_a h) \sum_{n_b=0}^{N_b-1} \exp(2\pi i n_b k) \sum_{n_c=0}^{N_c-1} \exp(2\pi i n_c l). \tag{18}$$

These summations can be explicitly performed and written in a compact form. For the summation along the a axis, for example, we find

$$\begin{aligned} \mathrm{S} \equiv \sum_{n_a=0}^{N_a-1} \exp(2\pi i n_a h) &= 1 + \exp(2\pi i h) + \exp(2\pi i h 2) \\ &+ \ldots + \exp[2\pi i h(N_a - 1)]. \end{aligned} \tag{19}$$

This shows that

$$\mathrm{S} - \mathrm{S}\exp(2\pi i h) = 1 - \exp(2\pi i h N_a), \tag{20}$$

and thus

$$\begin{aligned} \mathrm{S} &= \frac{1 - \exp(2\pi i h N_a)}{1 - \exp(2\pi i h)} \\ &= \frac{\exp(\pi i h N_a)[\exp(-\pi i h N_a) - \exp(\pi i h N_a)]}{\exp(\pi i h)[\exp(-\pi i h) - \exp(\pi i h)]} \\ &= \frac{\exp(\pi i h N_a)\sin(\pi h N_a)}{\exp(\pi i h)\sin(\pi h)}. \end{aligned} \tag{21}$$

The other summations can be done analogously, and therefore we obtain for the scattering amplitude

$$\Phi(\mathbf{Q}) \frac{\sin(\pi N_a h)}{\sin(\pi h)} \frac{\sin(\pi N_b k)}{\sin(\pi k)} \frac{\sin(\pi N_c l)}{\sin(\pi l)}, \tag{22}$$

where we grouped the phase factors in $\Phi(\mathbf{Q})$:

$$\Phi(\mathbf{Q}) = \frac{\exp(\pi i N_a h)}{\exp(\pi i h)} \frac{\exp(\pi i N_b k)}{\exp(\pi i k)} \frac{\exp(\pi i N_c l)}{\exp(\pi i l)}. \tag{23}$$

This phase factor depends on the choice of origin, but disappears when we compute the intensity by multiplying the amplitude by its complex conjugate. Including the integral over the unit cell, we find for the intensity

$$I(\mathbf{Q}) = r_e^2 |F(\mathbf{Q})|^2 \frac{\sin^2(\pi N_a h)}{\sin^2(\pi h)} \frac{\sin^2(\pi N_b k)}{\sin^2(\pi k)} \frac{\sin^2(\pi N_c l)}{\sin^2(\pi l)}. \tag{24}$$

This function has *very* sharp maxima when all diffraction indices have integer values. These maxima have values proportional to $(N_a N_b N_c)^2$. The widths of the peaks are proportional to $1/N$ along the three crystallographic directions, leading to an integrated intensity that is proportional to $N_a N_b N_c$, *i.e.* proportional to the volume of the crystal. The fact that significant intensity is only found when *all* diffraction indices are integer means that the momentum transfer, equation (16), is a reciprocal-lattice vector $\mathbf{G}$:

$$\mathbf{G} = H\mathbf{a}^* + K\mathbf{b}^* + L\mathbf{c}^*, \tag{25}$$

where H, K and L are integer. (For clarity, we will thus use lower-case diffraction indices when these are meant to have real values, and upper-case when they are integer.) This also implies that the angles of the wavevectors with respect to the specific lattice plane (HKL) follow Bragg's law. Bragg's law is thus a consequence of the fact that strong intensity only occurs when the contributions of all unit cells are in phase and is not a

pre-condition of the calculation. These consequences are shown here for the example of a crystal with parallelepiped shape, but remain valid for any crystal shape.

X-ray diffraction is frequently explained by considering the reflection of X-rays from a series of equally spaced planes with uniform intensity. This is a convenient way to derive Bragg's law, but does not properly describe the physics of the scattering process. First of all, X-rays are *not* reflected from planes, but induce scattering from all atoms in the crystal and in all directions. The scattering from individual atoms is very weak, and thus only significant intensity occurs when the contributions of all unit cells are in phase. For a reflection HKL the condition that all contributions should be in phase is equivalent to the condition that the incoming and outgoing angles of the X-ray beams with respect to the (HKL) plane are equal, and thus this corresponds to a 'reflection'. Secondly, the scattering centres are not distributed uniformly in a plane, but are discrete atoms arranged in a periodic lattice. For a correct calculation of the phase of each contribution, it is important to take this discrete nature into account, as was done in the derivation above.

We can, nevertheless, easily derive the scattering amplitude in the case of planes with uniform electron density. We assume the plane to be along the a and b directions. The summation over lattice points we performed above is replaced by an integral. For the a direction, this becomes

$$\int_{-L_a/2}^{L_a/2} \exp(2\pi i h x)\,\mathrm{d}x = \frac{\exp(2\pi i h x)}{2\pi i h}\Big|_{-L_a/2}^{L_a/2} = \frac{\sin \pi h L_a}{\pi i h}, \quad (26)$$

where L_a is the length of the plane in the a direction in fractional units. The amplitude of the full system is thus

$$A_{\text{planes}}(\mathbf{Q}) = r_e F(\mathbf{Q})\Phi(\mathbf{Q}) \frac{\sin(\pi L_a h)}{\pi h} \frac{\sin(\pi L_b k)}{\pi k} \frac{\sin(\pi N_c l)}{\sin(\pi l)}. \quad (27)$$

Compared with the amplitude when the 3D lattice is included, the denominators for the h and k terms no longer have the sine function. With the continuous planes, Bragg peaks only occur at $h = k = 0$; the others are absent, because no periodicity is included along the in-plane directions. It is somewhat unnatural to use a description in which there is a difference between the three crystallographic axes, because diffraction behaves the same in all directions. Nevertheless, the result when using the uniform plane approach is a good approximation when considering the scattering in the specular direction and its immediate vicinity.

In the main part of the paper, we compare the results of this conventional approach with those presented in F14. Since F14 uses the uniform plane approximation, we will do this as well. F14 also uses a 2D system, and it is straightforward to adapt our 3D result to this. By leaving out the c direction (l in reciprocal space), this result is valid for the 2D case when we swap b and c. The situation is sketched in Fig. 7. In order to be comparable with F14, we leave out the unimportant phase factors and also ignore the pre-factors in the amplitude, as

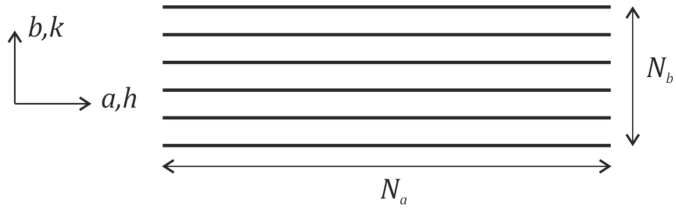

Figure 7
The 2D geometry considered in F14, using continuous planes (or lines in the 2D case) to represent the crystal lattice in the lateral direction.

these are not important for this comparison. The result of conventional diffraction theory for the 2D case is then

$$A'(h,k) = \frac{\sin(\pi N_a h)}{\pi h} \frac{\sin(\pi N_b k)}{\sin(\pi k)}. \quad (28)$$

A2. Conversion to angles

The amplitude in equation (28) is expressed in terms of (real) diffraction indices, which is a compact way of describing a position in reciprocal space. Each point (h, k) corresponds to a specific scattering geometry. F14 uses incoming and outgoing angles with respect to the scattering planes and therefore we will now convert equation (28) to angular coordinates.

Following F14, we use for the incoming angle the symbol Ω. The total scattering angle is fixed at 2θ, which may have a value corresponding to a Bragg reflection or not. The geometry is shown in Fig. 1. We can write the incoming and outgoing wavevectors as the following 2D vectors:

$$\mathbf{K}_{\text{in}} = \frac{2\pi}{\lambda} \begin{pmatrix} \cos\Omega \\ -\sin\Omega \end{pmatrix} \quad (29)$$

and

$$\mathbf{K}_{\text{out}} = \frac{2\pi}{\lambda} \begin{bmatrix} \cos(2\theta - \Omega) \\ \sin(2\theta - \Omega) \end{bmatrix}. \quad (30)$$

For the momentum transfer we then find

$$\mathbf{Q} = \mathbf{K}_{\text{out}} - \mathbf{K}_{\text{in}} = \frac{2\pi}{\lambda} \begin{bmatrix} \cos(2\theta - \Omega) - \cos\Omega \\ \sin(2\theta - \Omega) + \sin\Omega \end{bmatrix} = \frac{2\pi}{a} \begin{pmatrix} h \\ k \end{pmatrix}. \quad (31)$$

The last term is $\mathbf{Q}$ written as a vector in reciprocal-space coordinates, and this yields

$$\begin{pmatrix} h \\ k \end{pmatrix} = \frac{a}{\lambda} \begin{bmatrix} \cos(2\theta - \Omega) - \cos\Omega \\ \sin(2\theta - \Omega) + \sin\Omega \end{bmatrix}. \quad (32)$$

A3. Crystal size

Fig. 4 showed the effect of the crystal shape on the residual intensity in reciprocal space. The relative intensity of the residual maxima strongly depends on the size of the crystals as well. Fig. 8 therefore shows the intensity for cubic and spherical crystals with different sizes (including the size used in the main text), normalized to a value of 1 at the Bragg peak. The figure shows that the relative intensity of the first secondary maximum is in all cases the same, but because the tails are

much steeper, the intensity at a specific distance from the Bragg peak is rapidly decreasing for increasing crystal size. This is true for both crystal shapes, but for the spherical crystal the decrease as a function of size is much more pronounced. The decrease scales with the ratio of area over volume, where the area is that part of the crystal surface that has the orientation along the corresponding direction in reciprocal space. For the cubic shaped crystal, the facets are large and thus the $h00$ direction shows the weakest decay in intensity. Non-facet directions show a much stronger decay, similar to the spherical crystal shape.

The sizes shown in Fig. 8 are much smaller than typical grains of a powder sample, which will have sizes of 10000 unit cells or more. The residual intensity is then less than $\sim 10^{-6}$ of the Bragg peak.

A4. Crystal termination and roughness effects

The effect of crystal termination and shape was demonstrated in the main text by considering the two special cases of a cubic or a spherical shape. These effects can be more generically shown by using the shape function $s(\mathbf{r})$ to describe the electron density of the crystal:

$$\rho(\mathbf{r}) = \left[\rho_u(\mathbf{r}) * \sum_{n_a,n_b,n_c} \delta(\mathbf{r} - \mathbf{R}_j)\right] s(\mathbf{r}). \tag{33}$$

$\mathbf{R}_j$ was given in equation (13). Using this approach, the total electron density is written as the convolution of the electron density of a single unit cell $\rho_u(\mathbf{r})$ with the crystal lattice which is written as an infinite series of Dirac delta functions. This is multiplied by the shape function, which has value 1 inside the crystal and 0 elsewhere. Inserting this in equation (12) gives

$$A(\mathbf{Q}) \propto \left[\sum_{HKL} F(\mathbf{Q})\delta(\mathbf{Q} - \mathbf{G})\right] * S(\mathbf{Q}) = \sum_{HKL} F_{HKL} S(\mathbf{Q} - \mathbf{G}), \tag{34}$$

where the pre-factors have been left out. This expression shows that the scattered amplitude is confined to points $\mathbf{G}$ in reciprocal space, with a weight given by the structure factor F_{HKL} and with a profile that is determined by the convolution with the Fourier transform $S(\mathbf{Q})$ of the shape function. The intensity at each reciprocal-lattice point will thus be proportional to $|F_{HKL}|^2$. As we already concluded above, the momentum transfer, equation (16), is strictly a reciprocal-lattice vector and the angles of the wavevectors with respect to the specific lattice plane (HKL) follow Bragg's law.

We first apply the shape function and its Fourier transform to a crystal with a cubic shape. For a crystal with size L_a, L_b and L_c along the three axes (all in fractional, dimensionless coordinates), the shape function can be written as

$$s(x, y, z) = \begin{cases} 1 & |x| \le L_a/2, |y| \le L_b/2, |z| \le L_c/2 \\ 0 & \text{otherwise.} \end{cases} \tag{35}$$

The Fourier transform along the x direction is then

$$\int_{-L_a/2}^{L_a/2} \exp(2\pi i h x)\,\mathrm{d}x = \frac{1}{2\pi i h}\exp(2\pi i h x)\Big|_{-L_a/2}^{L_a/2} = \frac{\sin \pi h L_a}{\pi i h}. \tag{36}$$

The y and z directions give equivalent results. This yields an amplitude that in essence is the same as in equation (22); only the sine in the denominator is not there [it is retrieved when doing a full summation over all lattice points (Vlieg, 2012), but that is unimportant here]. L_a is the same as N_a if we assume its value is an integer. Using the shape function, we thus reproduce the result, equation (24), of the lattice summation we performed earlier.

Using the relation between shape function and its Fourier transform, we can now directly understand the effect of surface roughness. The cubic shape we just discussed corresponds to a *step* function along six directions and thus gives a relatively broad Fourier transform. However, facets of a typical crystal are not perfectly flat, but have a roughness, corresponding to a *broader* profile in real space. This means that the Fourier transform will be *sharper*, thus the tails become rapidly weaker away from the Bragg reflection.

The spherical shape can in principle also be treated using the shape function. We then need to compute the Fourier transform of a sphere, which, because of its abrupt termination, yields weak, spherical fringes in reciprocal space. For an irregular crystal shape, without significant facets and with surface roughness, the peak profile in reciprocal space becomes very sharp and the intensity away from the Bragg

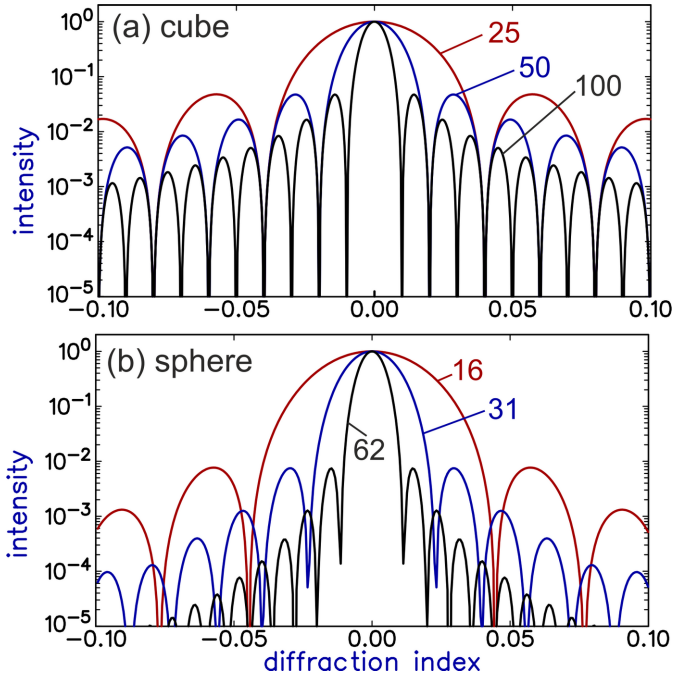

Figure 8
The normalized intensity profile of crystals with a cubic and with a spherical shape, for three different sizes: cubes with 25, 50 and 100 unit cells, and spheres with a radius of 16, 31 and 62 unit cells, chosen to have nearly the same volume as the cubes. The larger the crystal, the more rapid the decay of intensity away from the Bragg peak. In all cases the intensity is shown along the $h00$ direction in reciprocal space.

peak becomes so weak that it cannot be distinguished from the background. The integrated intensity of such a Bragg peak is thus a well defined quantity.

As we saw, the exact profile of a reflection depends on several details, and crystal termination is one of them. The fact that a sharply truncated crystal leads to extra intensity away from the main Bragg peaks is applied in surface X-ray diffraction (Robinson & Tweet, 1992; Vlieg, 2012), where crystal truncation rods (Robinson, 1986) represent the weak intensity tails emanating from Bragg peaks with a direction perpendicular to the surface. We can also use the shape function for this case. In surface diffraction, however, only one interface is normally probed, the other is so far away that the X-rays cannot reach this due to absorption. This can be accounted for by adding a (dimensionless) attenuation length Λ to the shape function. Following the convention in surface diffraction, we choose the z direction in real space (and the l direction in reciprocal space) for $s(z)$ to compute the scattering amplitude:

$$s(z) = \begin{cases} \exp(z/\Lambda) & z \leq 0 \\ 0 & z \geq 0. \end{cases} \tag{37}$$

This gives for the Fourier transform:

$$\begin{aligned} &\int_{-\infty}^{0} \exp(z/\Lambda)\exp(2\pi i l z)\,\mathrm{d}z \\ &= \frac{1}{1/\Lambda + 2\pi i l}\exp(z/\Lambda)\exp(2\pi i l z)\Big|_{-\infty}^{0} \\ &= \frac{1}{1/\Lambda + 2\pi i l} \approx \frac{1}{2\pi i l}. \end{aligned} \tag{38}$$

Each reflection thus obtains tails of intensity that decay as $1/l$. The fact that now only one interface plays a role means that no interference fringes occur, but only tails of monotonically decaying amplitude. The effect of Λ is only significant for l values very close to a bulk reflection, and is therefore often ignored (as in the rightmost part of the equation). The intensity for this crystal truncation rod for the case of an area of 50×50 unit cells (*i.e.* the cubic crystal we considered earlier) is plotted together with the cubic case in Fig. 9. We see that the decay follows that of the cubic, flat crystal. The local maxima of the cubic crystal are a factor 4 higher, because of the constructive interference of the amplitude of two interfaces for that case, compared with the amplitude of a single interface of the crystal truncation rod. The fact a single interface gives residual intensity in reciprocal space in the form of a crystal truncation rod shows that it is better to consider the residual intensity as a crystal termination effect, rather than a finite-size effect. For small crystals, the effects of two interfaces may lead to fringes, but that is not typical for crystal grains.

Typical surfaces are not perfectly flat, thus do not have the step profile given in equation (37). A mathematically convenient way to introduce surface roughness is to have an exponentially decaying roughness, characterized by a decay length ζ (in fractional, dimensionless coordinates). The shape function then becomes

$$s_{\mathrm{rough}}(z) = \begin{cases} \exp(z/\Lambda) & z \leq 0 \\ \exp(-z/\zeta) & z \geq 0. \end{cases} \tag{39}$$

Straightforward mathematics then yields for the amplitude along the l direction

$$A(l) = \frac{1}{2\pi i l(1 - 2\pi i l\zeta)}, \tag{40}$$

where we again ignored the effect of the attenuation length Λ. The intensity is thus

$$I(l) = \frac{1}{4\pi^2 l^2(1 + 4\pi^2 l^2\zeta^2)}. \tag{41}$$

Fig. 9 shows an example of the reduced intensity along a crystal truncation rod for $\zeta = 4.8$, a value chosen to show a significant effect. The intensity decrease becomes more pronounced for increasing distance from the Bragg reflection. In surface X-ray diffraction one aims to measure intensity along the full crystal truncations rods, and thus it is important that the surface is as smooth as possible. A root-mean-square roughness of a few Å already makes it impossible to measure full crystal truncation rods. Also for nearly flat surfaces the intensity is weak (about a factor 1 million less than for bulk reflections) and thus synchrotron radiation sources are used to measure such rods and derive the surface structure from the integrated intensity. Crystals for which a surface is not specially prepared have no significant intensity tails, and this will be the case for typical grains of a powder sample.

A final point on the crystal termination concerns dynamical diffraction (Batterman & Cole, 1964). When deriving the diffracted intensity from a perfect (and large) crystal, multiple scattering plays a dominant role close to the Bragg condition and thus needs to be taken into account. (The Bragg angle in dynamical scattering differs slightly from that according to Bragg's law because of refraction effects.) The theory shows that total scattering occurs over a very narrow angular range, beyond which the intensity rapidly decreases. These intensity tails show the same $1/l^2$ dependence that we found for crystal

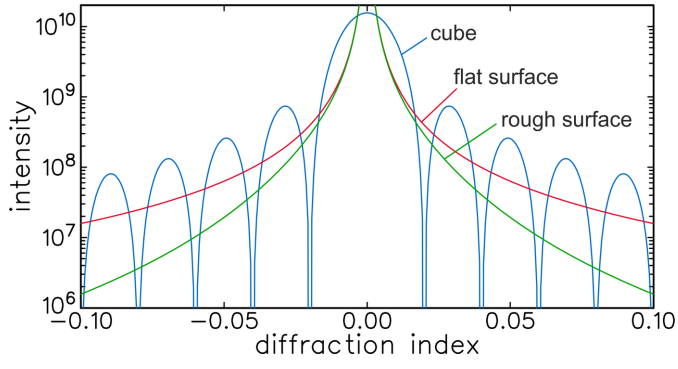

Figure 9
A comparison of the intensity from a cube-shaped crystal with that computed for a flat and a rough surface. The smooth curves are called crystal truncation rods in the context of surface diffraction. Roughness leads to a decrease in intensity.

truncation rods. This is as expected, because in the dynamical theory a flat surface is explicitly taken into account. The effects of multiple scattering rapidly decrease away from the Bragg condition and then the intensity becomes the same as that computed using the kinematic theory.

References

Batterman, B. W. & Cole, H. (1964). *Rev. Mod. Phys.* **36**, 681–717.
Cowley, J. M. (1984). *Diffraction physics*. Amsterdam: North-Holland.
Fewster, P. F. (2014). *Acta Cryst.* A**70**, 257–282.
Fewster, P. F. (2018*a*). *Acta Cryst.* A**74**, 457–465.
Fewster, P. F. (2018*b*). *Acta Cryst.* A**74**, 481–498.
Fewster, P. F. (2023). *Crystals*, **13**, 521.
Fraser, J. T. & Wark, J. S. (2018). *Acta Cryst.* A**74**, 447–456.
Giacovazzo, D. (2011). *Fundamentals of crystallography*. Oxford University Press.
Guinier, A. (1994). *X-ray diffraction in crystals, imperfect crystals, and amorphous bodies*. New York: Dover.
Hammond, C. (2015). *The basics of crystallography and diffraction*. Oxford University Press.
Robinson, I. K. (1986). *Phys. Rev. B*, **33**, 3830–3836.
Robinson, I. K. & Tweet, D. J. (1992). *Rep. Prog. Phys.* **55**, 599–651.
Vlieg, E. (2012). *Surface and interface science*, Vol. 1, *Concepts and methods*, edited by K. Wandelt. Wiley.
Warren, B. E. (1990). *X-ray diffraction.* Dover.